symmetry

MDPI

Article

Simplified Procedure for Capacity Check of Historic Monolithic Glass Windows under Soft-Body Collision/Bird-Strike

Chiara Bedon [1,*] and Maria Vittoria Santi [2]

[1] Department of Engineering and Architecture, University of Trieste, 34127 Trieste, Italy
[2] Polytechnic Department of Engineering and Architecture, University of Udine, 33100 Udine, Italy
* Correspondence: chiara.bedon@dia.units.it; Tel.: +39-040-558-3837

Abstract: Differing from present structural design procedures, most of the existing glass windows and even historic components in traditional/old buildings are not specifically designed to resist possible accidental loads. Rather thin monolithic ordinary annealed glass panels can be found in vertical non-structural envelopes, where they are often arranged to cover large surfaces. As such, an accidental glass fracture could originate even from rather common and moderate impact events and result in severe risk for people, due to propagation of dangerous shards from these vulnerable and fragile building components. To assess potential risks and support possible mitigation strategies, the present study is focused on the bird-strike analysis of existing/historic linearly restrained non-structural glass windows, based on a parametric Smoothed-Particle Hydrodynamics (SPH)–Finite Element (FE) model. Starting from a 1 m–wide and 1.5 m–high configuration, the attention is first given to various influencing parameters, such as impactor features (mass, 0.35–1.81 kg; impact speed, 0–40 m/s; and, thus, impact energy) and the target window (glass thickness, 4–6 mm; impact point; and, thus, glass stiffness). Local and global effects due to parametric localized bird-strikes are discussed based on non-linear dynamic numerical analyses and in terms of expected deflections, tensile stress peaks, and damage extension/severity (i.e., D1 to D3 damage levels). Scale effects are also examined for a case-study historic envelope (≈7 m in total size, 5 mm in thickness), and one of its 2.58 m × 3.3 m large glass components. Furthermore, a simplified empirical approach based on analytical formulations and normalized charts is proposed for a preliminary vulnerability assessment of historic monolithic glass envelopes, including parameters to account for impactor features and glass panel size/thickness, based on vibration-frequency considerations.

Keywords: soft-body impact; bird-strike; glass; windows; Finite Element Analysis (FEA); Smoothed-Particle Hydrodynamics (SPH) modeling

Citation: Bedon, C.; Santi, M.V. Simplified Procedure for Capacity Check of Historic Monolithic Glass Windows under Soft-Body Collision/Bird-Strike. *Symmetry* **2022**, *14*, 2198. https://doi.org/10.3390/sym14102198

Academic Editor: Jan Awrejcewicz

Received: 18 September 2022
Accepted: 13 October 2022
Published: 19 October 2022

1. Introduction

Bird-strike analysis and damage prediction is a design issue of primary relevance for aircraft engineering applications, where wings or fuselage components may suffer for possible collision during flying stage and take the form of serious structural damage [1]. From a practical point of view, the Federal Aviation Regulations (FAR, [2]) provides reference performance indicators for forward-facing components and requires dedicated bird-strike resistance assessment (generally based on certification test protocols). Over the years, various research studies have been dedicated to this problem. Experiments can be found, for example, in References [3,4], while a multitude of numerical simulations have been presented in the years to extend/support complex experimental protocols (see References [5–10] and others). A common aspect of several aircraft-related studies was the evidence of severe vulnerability for mechanical aircraft components, but also for glass elements.

In this paper, based on extensive feedback from the literature, the attention is given to the soft-body collision/bird-strike analysis of simple glass windows that are not specifically

designed to sustain design mechanical loads and could represent a potential risk for occupants. The simplest glass window, in use several years ago but still present in old buildings, consists, in fact, of a thin monolithic glass panel like the one shown in Figure 1. The use of metal, timber, or polycarbonate frames allows us to cover surfaces with modular units with a typical thickness of 3 to 4 mm.

Figure 1. Examples of ordinary monolithic glass windows.

For newly designed glass components in buildings, several technical documents and guidelines are nowadays available to support structural designers in preventing possible damage and failure of variably restrained glass panels under ordinary design actions [11], as well as from wind [12–14], seismic loads [15–18], impact due to crowd/human bodies [19–22], or even explosions and multi-hazard [23–27] and debris [28]. A basic assumption is the use of (minimum) double-laminated glass sections to improve safety levels even in case of fracture.

However, this is not the case for existing/historic glass components in windows and envelopes, which are typically composed of ordinary annealed float glass and are, thus, highly vulnerable (see, for example, Reference [20]). Most importantly, their residual capacity and safety-level analysis or vulnerability measure is more complex and uncertain, thus making more difficult the subsequent definition of possible mitigation strategies, where required [29]. This vulnerability is expected to increase with the size and flexibility of glass panels, as it is in case of large covered surfaces), due to the typically low tensile strength in bending for annealed glass material and thus reduced capacity to withstand collisions [30,31].

Ordinary historic windows composed of annealed monolithic glass (and not specifically designed as load-bearing building components) are hence taken into account in this paper. Major efforts of numerical analyses are spent on the assessment of the impact response of linearly restrained monolithic window panels under bird-strike scenarios. While very rigid multi-laminated glass panels of modern facades under small-size bird-strike represent a risk for birds, and specific bird-friendly design codes should be possibly taken into account [32], thin monolithic glass panels of historic windows and envelopes may suffer damage under impact. As such, a major risk could be expected in terms of possible glass fracture and consequent injuries in building customers. The overall investigation herein presented was inspired by a case study of an in-service glass envelope constructed in Italy in 1962, in the form of a large-size envelope of a museum (Section 2) and subjected to rather frequent bird-strikes.

The presently discussed parametric numerical analyses were carried out with the support of Smoothed-Particle Hydrodynamics (SPH)–Finite Element (FE) numerical models [33] developed in ABAQUS/Explicit [34] (see Section 3). A set of accidental scenarios is taken into account and numerically explored by changing the impact parameters (i.e., mass, size, and impact speed of soft-body impactor or impact point), as well as the mechanical properties of glass panels (and thus their bending stiffness and accommodation to local impact phenomena). Differing from conventional soft-body impactors of typical use for

the certification and assessment of glass facades (i.e., double twin-tyre or spheroconical bag impactors [35,36]), the effect and potential risk due to relatively small impactors with a specific viscous behavior under collision are discussed in Section 4. Furthermore, simple empirical analytical expressions and normalized charts validated toward the presented SPH–FE models are proposed in Section 5 as an efficient tool for the practical derivation of preliminary vulnerability considerations. A major advantage of the presented simplified procedure, as shown, is that the expected damage severity/extension can be estimated for a given monolithic glass panel, with linear restraints along the edges, when subjected to localized bird-strike. Possible mitigation strategies and even more sophisticated numerical simulations can be taken into account to minimize risks for customers, where required.

2. Background

The present numerical investigation took inspiration from a case-study system consisting of a steel–glass envelope designed in 1961 and built up in 1962 as a composition of glass panes and a grid of steel mullions and arched transoms (Figure 2a). The facade belongs to the so-called Information and Documentation Centre (CID) museum [37], which is located in Torviscosa (Udine, Italy). The particular aspect of this system is represented by its shape (circle-based facade concept) and by its size, characterized by approximately 7 m of diameter (see Figure 2b, with dimensions in cm), which is relatively large compared to the thickness of annealed glass components (5 mm each). Glass elements are, in fact, shaped to follow the overall circle path of the facade and are characterized by simple monolithic (and relatively small) total thickness, as compared to the covered surface. Moreover, steel members are reduced to a minimum in order to preserve the transparency of the facade. The maximum size of the central glass panel, more precisely, was measured to be 3.3 m in height by 2.58 m in width. The total mass of steel and glass members amounts approximately M_{TOT} = 2358 kg, with a minimum contribution for glass in the order of ≈0.13 M_{TOT} (≈309 kg).

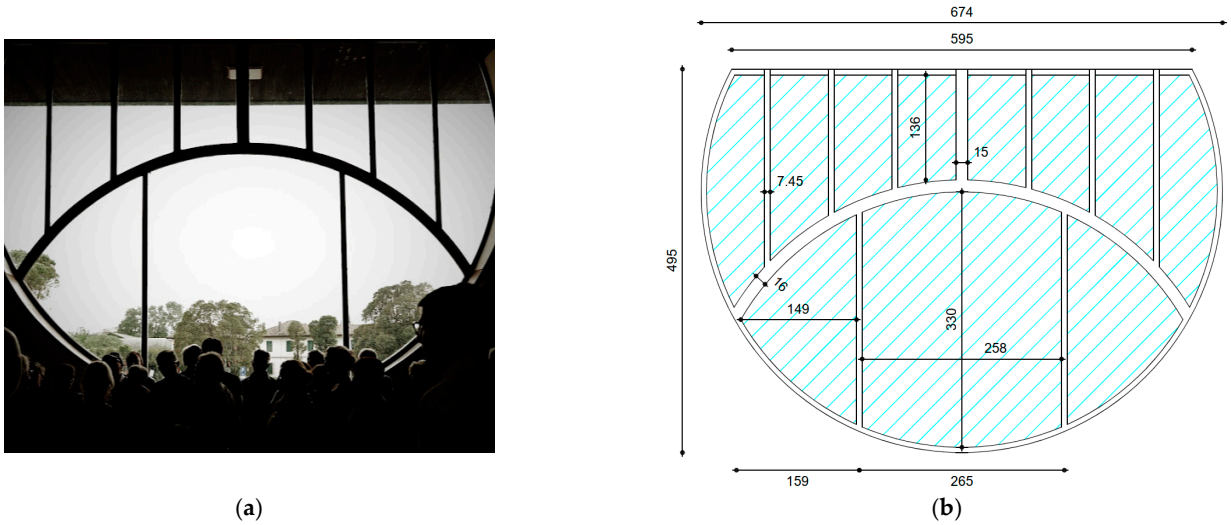

(**a**) (**b**)

Figure 2. *Cont.*

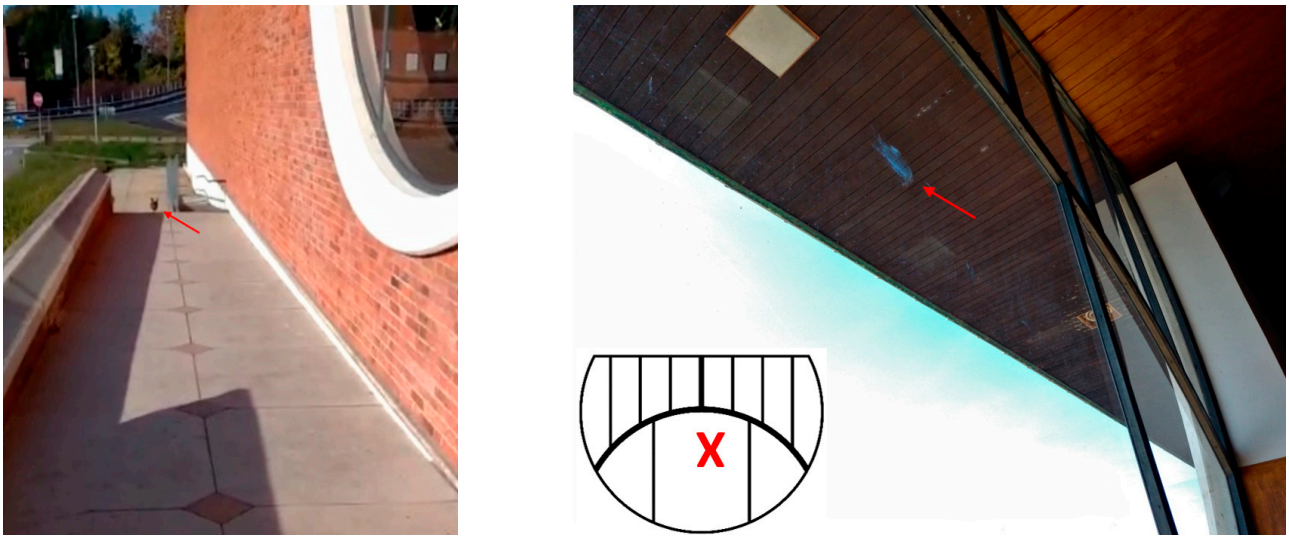

(**c**) (**d**)

Figure 2. Example of historical round-shaped facade: (**a**) front view and (**b**) schematic layout with dimensions in cm, with (**c**,**d**) in-field evidences of accidental bird-strike (October 2021).

The steel–glass system is not freely accessible to visitors/occupants, thus there is no risk of failure due to crowd loading. However, during normal service conditions, there are several sources of vibrations for glass. The construction site and the building are very close to an industrial plant, and, thus, they are subjected to daily heavy traffic of trucks and cars. Moreover, a railway track (Trieste-Venezia path) runs parallel to the building (north side), at a distance of few meters. Finally, the glass facade (on the south side) is subjected to wind gusts and rather frequent accidental strikes by birds (Figure 2c,d), thus suggesting the need of additional detailed investigations for vulnerability purposes. Typical accidental strikes for glass were found that were characterized by impact of pheasants (*Phasianus colchicus* type [38], noted as "B#1" impactor, in the following), as shown in Figure 3a, or pigeons (*Columba livia* type [39]), as shown in in Figure 3b. Average impact conditions are summarized in Table 1 in terms of impactor mass, M, and impact energy, E_{imp} (range values):

$$E_{imp} = \frac{1}{2} M v^2 \quad (1)$$

where v is the impact speed (up to ≈20 m/s and ≈40 m/s for B#1 and B#2).

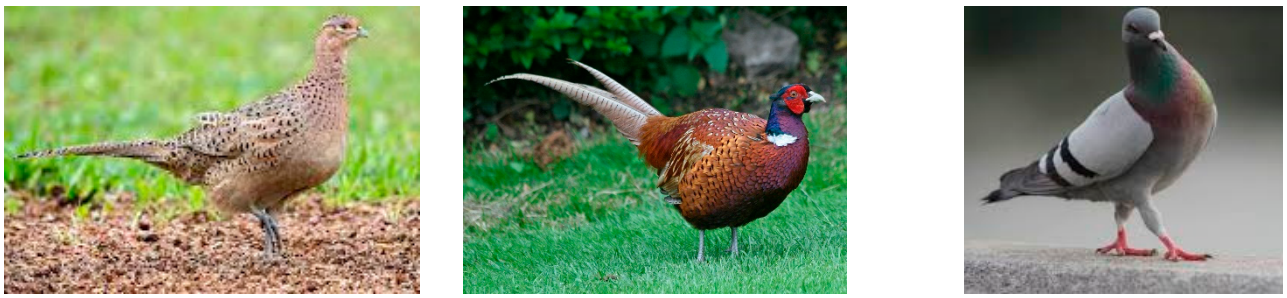

(**a**) (**b**)

Figure 3. Reference (**a**) B#1 (*Phasianus colchicus*) and (**b**) B#2 (*Columba livia*) soft-body impactors for the present study (out of scale).

Table 1. Summary of bird-strike features for the case-study system in Figure 2, with expected impact energy from Equation (1), based on average speed values from References [38,39].

Impactor Type	M (kg)	E_{imp} (J)
Pheasant (*Phasianus colchicus*)	1.3–1.81	260–360
Pigeon (*Columba livia*)	0.25–0.38	200–300

3. SPH–FE Numerical Investigation

3.1. Modeling Strategy

The SPH–FE numerical investigation in support of bird-strike vulnerability assessment of ordinary glass windows was carried out in ABAQUS/Explicit. In doing so, the bird impactor was described in the form of SPH body, while the structural model of target glass window was assembled in the form of a conventional FE model. For the collision scenarios of interest for the present study, the mass of birds, M, was comprised between 0.35 and 1.81 kg, while the imposed impact speed was assumed to be a maximum of v = 40 m/s, as also specified in Section 4.

Nowadays, commercial software packages offer various options for modeling the effect of bird collisions on structural components. Maximum effects can be, for example, predicted based on FE numerical approaches according to unpractical Lagrangian description of bird bodies, but such a method is often inaccurate for bird-strike applications and unpractical due to distortion phenomena [8,40]. The herein adopted SPH approach has the intrinsic meshless feature. Simulations discussed in Reference [33] for various configurations and collisions on rigid plates or tapered plates proved the accuracy of SPH method for bird-strike events. Many other applications, especially for aircraft components, can be found in the literature, such as References [41–44] and others. In those conditions, typically explored impact velocities were set in the range of ≈50–400 m/s [45]. Gelatin bird-like impactors for high-speed collision set up on three different rigid plates were experimentally and numerically investigated in Reference [46], based on SPH models. Diversely, the SPH method has been efficiently applied (on the side of structure) to a variety of structural components under low-velocity rigid-body impact [47–49] to explore a collision-speed range, v, from a minimum of ≈1 m/s up to ≈10 m/s.

Alternatively, the mesh-dependent, time-expensive, fixed boundary Coupled Eulerian–Lagrangian (CEL) approach can be used for accurate bird-collision studies [50]. Among others, parametric simulations can be found in Reference [51] for a composite wing under bird-strikes characterized by various impact angles and an imposed contact speed of v = 66 m/s. A promisingly efficient alternative approach to the classical CEL method is represented by the movable Eulerian domain option, in which the Eulerian volume is not fixed in space but can move and allow a strong reduction in mesh refinement and computational time, as also adopted in Reference [52].

3.2. Glass Panel

For each examined configuration, the FE structural model of the target window was composed of B = 1 m × H = 1.5 m monolithic shell elements (S4R type) to reproduce the nominal thickness of glass (t). Ideal nodal restraints were distributed along the edges to reproduce a clamp connection (for the glass-to-frame constraint, as in Figure 1), and the parametric analysis was run to take into account various glass thicknesses (t = 4, 5, and 6 mm) and dimensions/aspect ratios for target panels (see Figure 4).

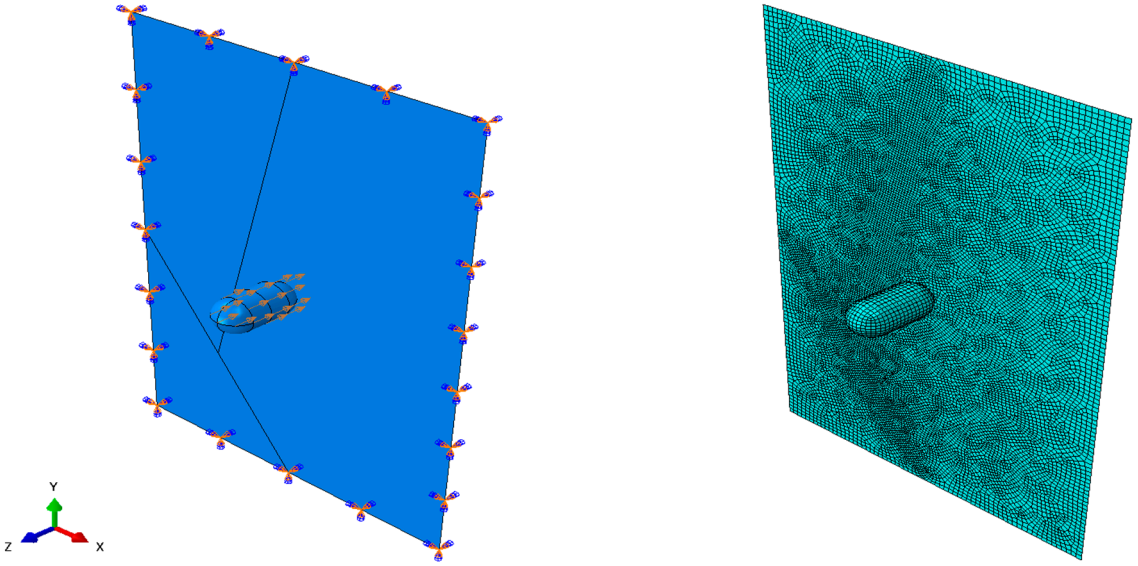

(**a**) (**b**)

Figure 4. Reference numerical model: (**a**) assembly and boundaries with (**b**) random mesh pattern for a typical SPH–FE bird-strike configuration (ABAQUS/Explicit).

In doing so, a free mesh pattern with a variable edge size was used, so as to preserve the accuracy of FE simulations and allow random propagation of cracks (if any). This resulted in a minimum edge size of 2 mm and a maximum of 20 mm, for a total of ≈19,500 elements and ≈110,000 Degrees of Freedom (DOFs).

The mechanical material characterization was based on experiments from the literature in order to account for the tensile brittle behavior of glass, as well as for possible strain rate effects under impact.

To this aim, a constitutive law was defined, with E_g = 70 GPa as the Young's modulus, ν_g = 0.23 as the Poisson' ration, and ρ_g = 2490 kg/m^3 as the material density [29–31], in combination with specific "damage initiation" and "damage evolution" parameters from ABAQUS/Explicit library, so as to characterize the damage variable, D (with $0 \leq D \leq 1$ and D = 1 denoting the loss of bearing capacity and fracture for the element). Figure 5a,b show the conventional stress σ-strain ε constitutive law from ABAQUS/Explicit user's guide that was adapted for the current investigations. It is worth noting that such a material model is specifically designed for the fracture of metals, but with justified calibration and validation fit for brittle elastic ceramics with strain-rate sensitivity effects, such as glass. A similar practical example can be found also in Reference [28] for the dynamic analysis of glass windows under debris impact. More in detail, the conventional constitutive law in Figure 5a is characterized by a first linear elastic response (OY path), which is governed by Young's modulus and yielding strength (in point Y). The conventional constitutive model allows us to then define the possible plasticity (YA path) and first "damage initiation" in point A. This is followed by "damage evolution" (AB path), which assumes that damage is characterized by the progressive degradation of the material stiffness, leading to failure, where final "erosion" with removal of failed elements from the original mesh can be also included (point B in Figure 5a).

In the present study, for glass material, a linear elastic behavior with tensile brittle failure was taken into account in simulations. A maximum principal stress criterion was taken into account for damage initiation. To this aim, with E_g = 70 GPa, the initial tensile strength for point Y was set to be equal to $\sigma_{g:k}$ = 45 MPa [29–31], as it is for annealed glass under quasi-static loads. The plastic stage (YA path in Figure 5a) was minimized to reproduce a brittle behavior in tension. This means that "damage initiation" was set to coincide with first exceedance of material strength (i.e., $\sigma_{g:k} = \sigma_Y = \sigma_A$). To this aim, under impact configurations, strain rate effects were taken into account based on a fracture

strength increase according to the Dynamic Increase Factor (DIF) trends of the literature (see for example [53]). Figure 5c reports the presently considered DIF evolution for annealed glass, for which the dynamic strength was calculated as follows:

$$\sigma_{g:k,DIF} = \sigma_{g:k} \cdot DIF \tag{2}$$

Such a DIF effect was numerically implemented for "damage initiation" in the form of equivalent fracture strain for glass, which was calculated under a linear elastic-behavior assumption as a function of strain rate, as follows:

$$\varepsilon_{g:fail,DIF} = \frac{\sigma_{g:k,DIF}}{E_g} \tag{3}$$

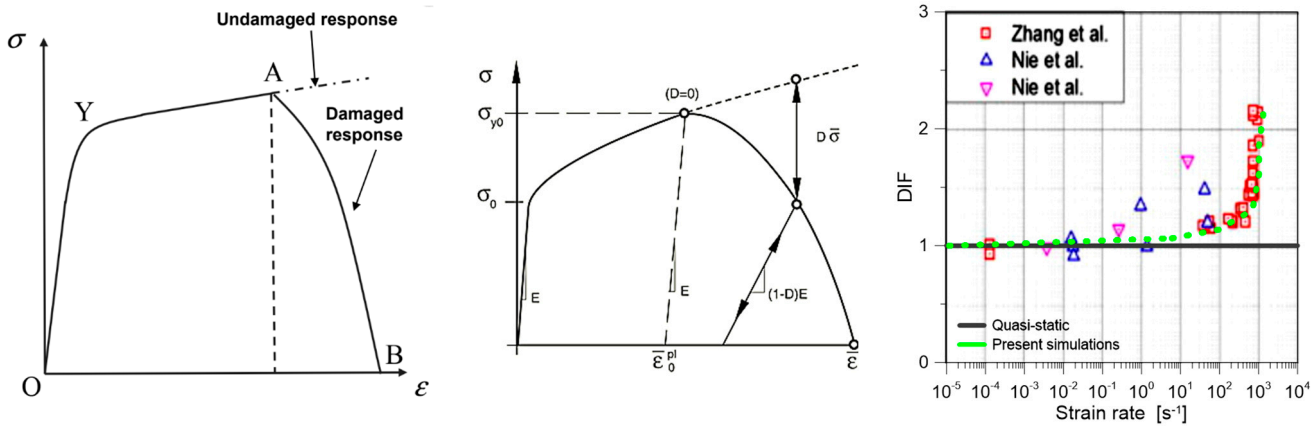

(**a**) (**b**) (**c**)

Figure 5. Mechanical characterization of glass material: (**a**,**b**) qualitative features of the conventional constitutive model herein adapted to account for glass damage (ABAQUS/Explicit); (**c**) reference DIF for glass in tension in present simulations.

Selected values taken into account for input definition are summarized in Table 2. Finally, the damaged response (AB path in Figure 5a) was implemented up to full stiffness degradation of fractured glass elements based on a reference fracture energy per unit area equal to $G_f = 3$ J/m^2 [54]. An "exponential" damage evolution was taken into account for the damage variable, with $0 \leq D \leq 1$. The "element deletion" option was also included in simulations, so as to remove failed glass elements during crack propagation.

Table 2. Summary of adopted parameters for input definition in present bird-strike simulations (ABAQUS/Explicit), based on Figure 5c—selected values—and Equations (2) and (3).

Strain Rate (s^{-1})	DIF (Figure 5c)	Fracture Strength (Equation (2)) (MPa)	Fracture Strain (Equation (3))
1.00×10^{-4}	1.00	45.00	6.429×10^{-4}
1.00×10^{-3}	1.00	45.00	6.429×10^{-4}
1.00×10^{-2}	1.01	45.45	6.493×10^{-4}
1.00×10^{-1}	1.02	45.90	6.557×10^{-4}
1.00	1.03	46.35	6.621×10^{-4}
1.00×10^{1}	1.04	46.80	6.686×10^{-4}
1.00×10^{2}	1.06	47.70	6.814×10^{-4}
1.00×10^{3}	1.14	51.30	7.329×10^{-4}
5.00×10^{3}	1.25	56.25	8.036×10^{-4}
1.00×10^{4}	1.55	69.75	9.964×10^{-4}
1.35×10^{4}	2.16	97.20	1.389×10^{-3}

3.3. SPH Bird

A cylindrical volume, with hemispherical ends like in Figure 6, was taken into account. The cylinder size was derived as a scaled shaped from Figure 6a, where the reported dimensions are representative of a conventional 1.81 kg bird [2]. So far, it is recognized that specific and more refined three-dimensional (3D) shapes should be considered for modeling bird collisions [55–57], due to local effects from shape of head, neck and torso of bird bodies during contact after impact. On the other side, the simplified cylinder shape—and its limits—is accepted as conventional volume shape in numerical simulations [9].

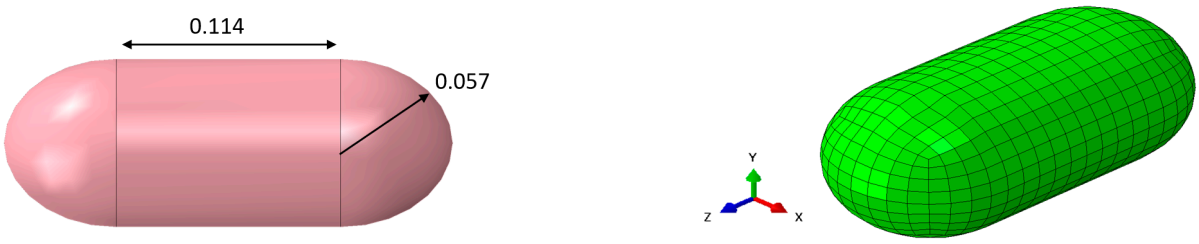

(**a**) (**b**)

Figure 6. Reference model detail: (**a**) nominal bird (values in meters, for 1.81 kg conventional size (B#1)) and (**b**) initial configuration for SPH bird model (ABAQUS/Explicit).

In the present study, the length to radius ratio was kept fix in 2:1, and the diameter d for impactors was in general defined as follows:

$$d = \sqrt[3]{\frac{24M}{3\pi\rho}} \tag{4}$$

with M as the total mass of the bird and ρ as its density.

To reproduce various strike configurations of technical interest, the cylindrical volume was assumed to hit perpendicularly the examined glass panels; that is, $\alpha = 90°$ the fixed impact angle. For each one of the strike conditions, an initial translational velocity, v, was assigned to the bird. To this aim, the impact effect on glass was investigated with the support of interposed "general" surface-to-surface penalty-based contact algorithm of ABAQUS/Explicit library, with frictionless behavior in the tangential direction and "hard" body behavior in the perpendicular direction. The mesh size and pattern, as in Figure 6b, were optimized based on preliminary analyses and resulted in around 2000 elements (C3D8R type). A time-based conversion of FE elements to SPH particles was included in "section controls" to have a simultaneous generation of particles. A single particle was generated per isoparametric direction (PPD = 1), with a distance less than 10 mm [44].

Regarding the material characterization, the major water composition of bird bodies was taken into account in the present simulations [9]. For each impact configuration, bird material was hence replaced with an equivalent volume of water, with input parameters as in References [5,58,59]. More precisely, the most important aspect in such a kind of hydrodynamic problem is that the material's volumetric strength and pressure are sensitive to the density ratio. The pressure-to-density relation is given by a linearly reduced Hugoniot expression:

$$p = \frac{\rho_0 c_0^2 \eta}{\left(1 - s_f \eta\right)^2}\left(1 - \frac{\Gamma_0 \eta}{2}\right) + \Gamma_0 \rho_0 E_m \tag{5}$$

where ρ_0 is the reference material density, Γ_0 and s_f are material constants, c_0 is the speed of sound in the material, and E_m is the internal energy per unit of mass. Moreover, $\eta = (1 - \rho_0/\rho)$ represents the nominal volumetric compressive strain, with ρ as the current material density, while the $(\rho_0 c_0^2)$ term is equivalent to the elastic bulk modulus at

small nominal strains. In the present simulations, the Mie–Gruneisen (Us-Up) equation of state (EOS) from ABAQUS/Explicit library was used for the hydrodynamic material characterization of bird bodies. The four input parameters for Us-Up EOS, according to Equation (5), were set as proposed in References [5,56,58–60]; that, is c_0 = 1480 m/s, s_f = 0, and Γ_0 = 0. While the Us-Up EOS is primarily used for shock simulations, studies from the literature proved its applicability (with herein reported input values) also for water-impact configurations under low-velocity collisions [61,62]. Finally, the material density was set as ρ_0 = 938 kg/m^3. Dynamic Newtonian viscosity was also considered for water fluid material and set to equal 0.001 Ns/m^2 [62]. This density value was kept constant through the parametric analysis, given that it depends on temperature only, and no temperature variations were taken into account.

3.4. Preliminary Validation

The FE structural and SPH bird models described in Sections 3.2 and 3.3 were preliminarily assessed and validated to verify their accuracy for parametric investigations. The attention was given to glass-panel features, as well as to bird parameters.

Among others, for the target glass panel, the effect of mesh size and pattern was first explored. The mesh size was found to have minor effects on impact performance assessment [44], especially in the elastic range. On the other side, for collapse configurations, both mesh size and pattern manifested major effects on numerical outcomes. As such, a variable mesh pattern like that shown in Figure 4b was finally privileged to facilitate (at least qualitatively) the evolution of free cracks of glass and to avoid less qualitatively realistic and mesh-dependent crack propagations (see also References [20,54,63,64]. In doing so, some selected glass windows were, in fact, subjected to bird-strike with different assigned speed amplitudes, v, at impact, so as to quantify the effect of mesh in terms of elastic response or even collapse and cracks. An example of investigated schemes is proposed in the selected mesh schemes of Figure 7.

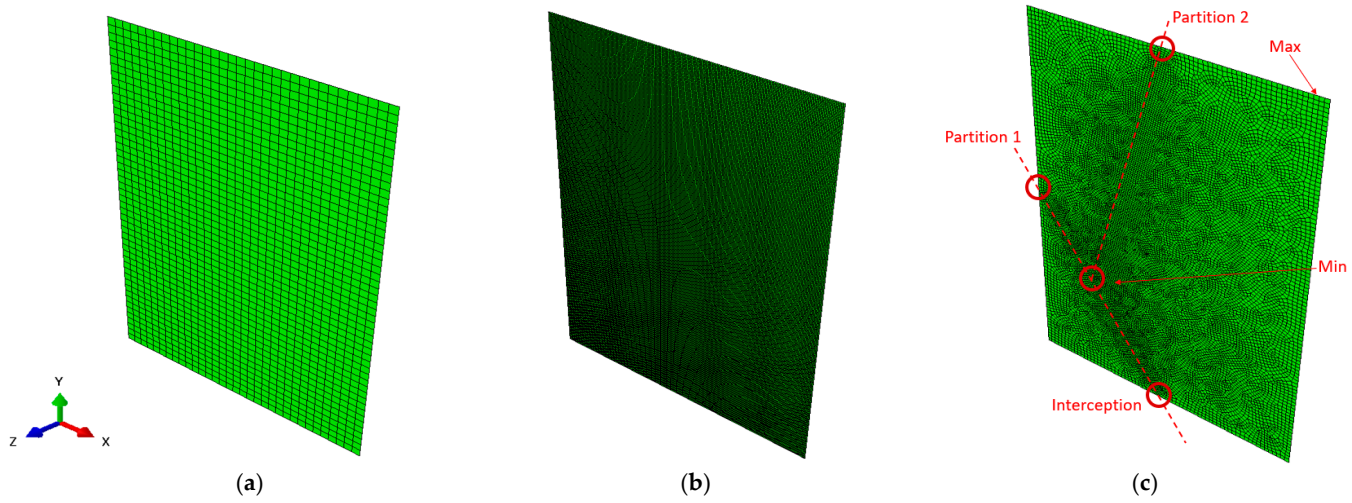

Figure 7. Example of mesh schemes in use for the sensitivity analysis (ABAQUS/Explicit): (**a**) 30 mm edge size model (≈10,500 elements and ≈54,000 DOFs), (**b**) 5 mm edge size model (≈64,000 elements and ≈376,000 DOFs), and (**c**) schematic approach for the optimization of current free mesh pattern.

Overall, the mesh sensitivity analysis first included some structured mesh schemes based on regular, 4-node S4R shell elements, and an edge size comprised between a maximum of 30 mm and a minimum of 1 mm for the uniform discretization of the target panel. The examples in Figure 7a,b refer to the 30 mm edge–size model (corresponding to ≈10,500 elements and ≈54,000 DOFs) and the 5 mm edge–size model (≈64,000 elements and ≈376,000 DOFs), respectively. The minimum edge size required to offer stable numerical outputs was detected on the base of a comparative analysis of the results in the

elastic and damaged scenarios. After this first step, various random mesh schemes were also addressed. Figure 7c schematizes the typical approach in use. The minimum edge size in the central part of glass panel ("Min") was selected from a sensitivity analysis for regular 4-node mesh schemes. A maximum edge size ("Max") was assigned along the perimeter of glass panel, based also on aspect-ratio considerations. To create variable mesh schemes and facilitate a non-symmetrical transition in the "Min–Max" range, two internal partitions were also defined, as schematized in Figure 7c. Basic parametric studies included changes in the interception points/inclination of these partitions, and the verification—for collapse configurations—of mesh-independent cracks randomly distributed and not aligned with initial partitions.

Comparative examples can be seen in Figure 8, where the "Current free mesh" model corresponds to Figure 4b assumptions (≈19,500 elements and ≈110,000 DOFs). More in detail, Figure 8a presents the out-of-plane displacement (Z-direction) in control point P1, under B#1 strike, with an imposed impact speed of v = 5 m/s. Such a configuration, for the examined glass panels, corresponds to linear elastic behavior. In Figure 8b, selected contour plots are proposed in terms of maximum principal stress distribution in glass. Finally, Figure 8c shows typical crack propagations—under identical bird-strike—with evidence of "structured" cracks or a random pattern.

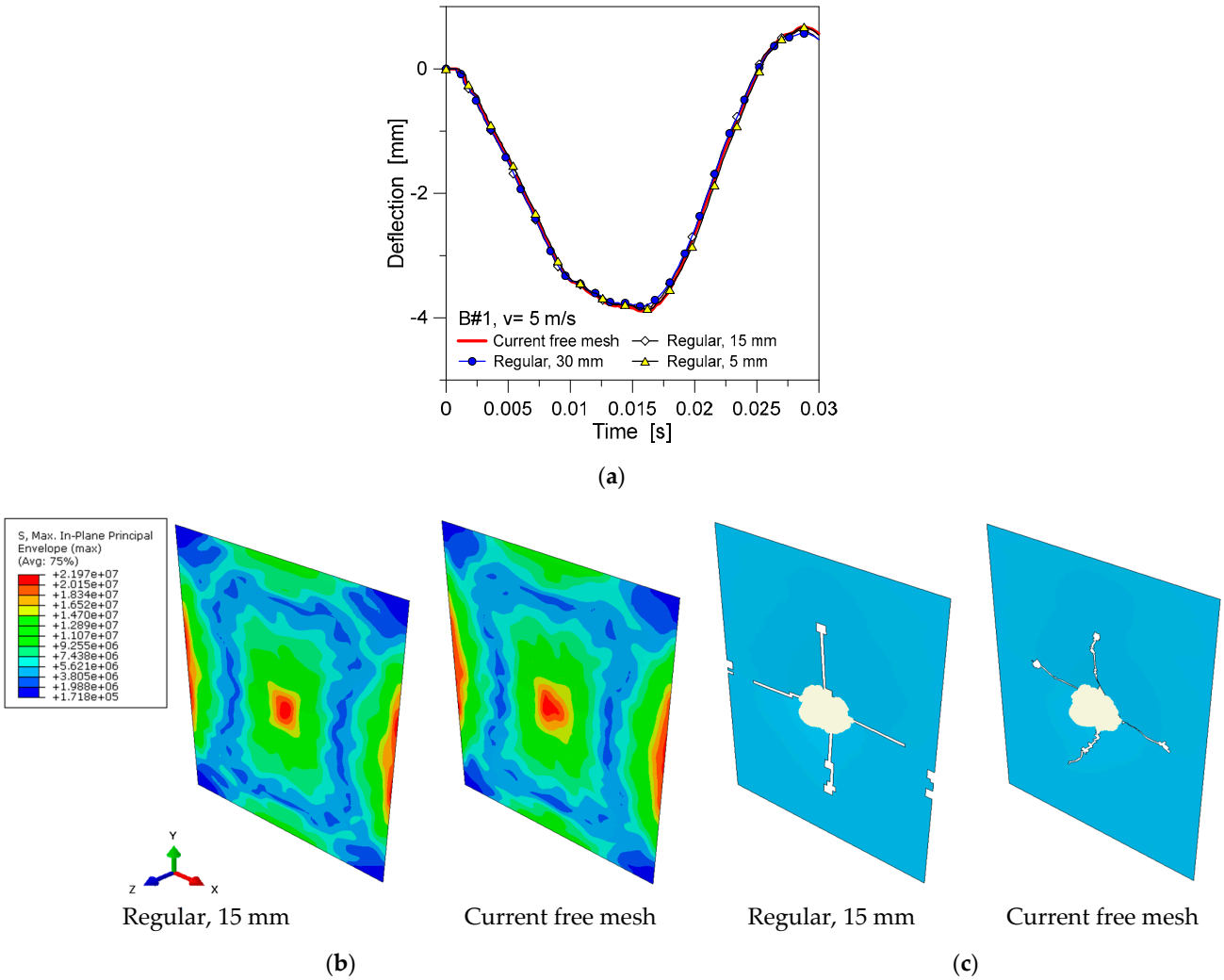

Figure 8. Preliminary mesh sensitivity analysis (selection): (**a**) deflection in time, with axonometric contour plots of (**b**) maximum principal stress distribution (unexposed side, legend in Pa), and (**c**) example of cracks for collapse configurations (ABAQUS/Explicit).

On the side of the glass panel, based on the "Current free mesh" pattern, the effect of the soft linear restraints along the edges was successively taken into account to replace ideally rigid supports, as shown in Figure 4a. To this, aim, a linear gasket support, as schematized in Figure 9a, was described in the form of 3D solid brick elements (with t_s = 5 mm of thickness and B_s = 40 mm of width for the tape) and connected to the perimetral elements of glass panel. The Young's modulus, E_s, of this supporting layer was initially set to be equal to $E_s = E_g$ = 70 GPa (that is E_s/E_g = 1) and successively reduced down to E_s/E_g = 0.0001.

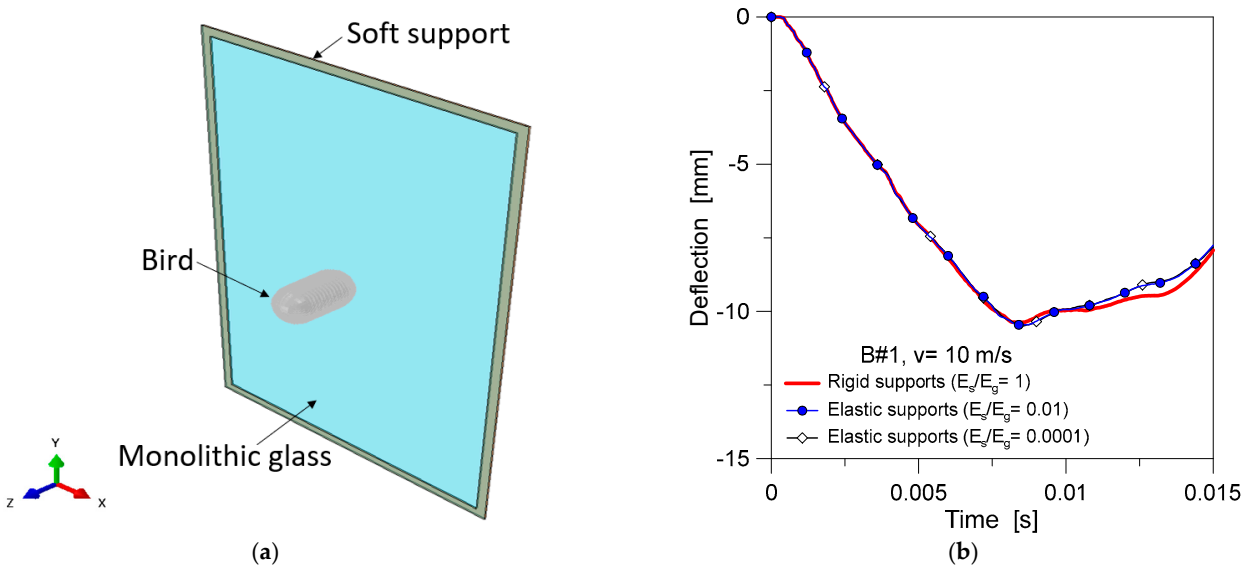

Figure 9. Preliminary bird-strike analyses: (**a**) monolithic glass panel with soft restraint at the edges (axonometric view); examples of (**b**) measured deflection at the center of glass (ABAQUS/Explicit).

For a given monolithic glass panel under B#1 impactor, with v = 10 m/s, the typical deflection history in the center of the panel is reported in Figure 9b. It can be noted that, under the effect of a localized bird collision, soft supports similar to present assumptions do not mitigate the glass panel from maximum impact effects in the target region, as also confirmed by the trend of monitored displacements. In other words, the use of simplified, ideally rigid linear supports for the present simulations does not significantly affect the dynamic response of examined systems.

Regarding the SPH bird model, preliminary attention was finally given to the assessment of such a modeling approach and its accuracy compared to the Coupled Eulerian–Lagrangian (CEL) modeling strategy, under the examined impact configurations (i.e., bird mass, M, and collision speed, v). To this aim, the modeling procedure and input calibration of the CEL bird components were carried out as performed in Reference [52]. Figure 10a shows an example of the assembled CEL model for the present assessment, with evidence of a monolithic shell glass panel and Eulerian part for bird-strike simulation. Typical deflection comparisons are reported in Figure 10b for a monolithic panel under the B#1 impactor (v = 10 m/s), as obtained from SPH or CEL bird-modeling strategies, respectively. It can be noted the rather good correlation of proposed deflection histories at the center of the glass.

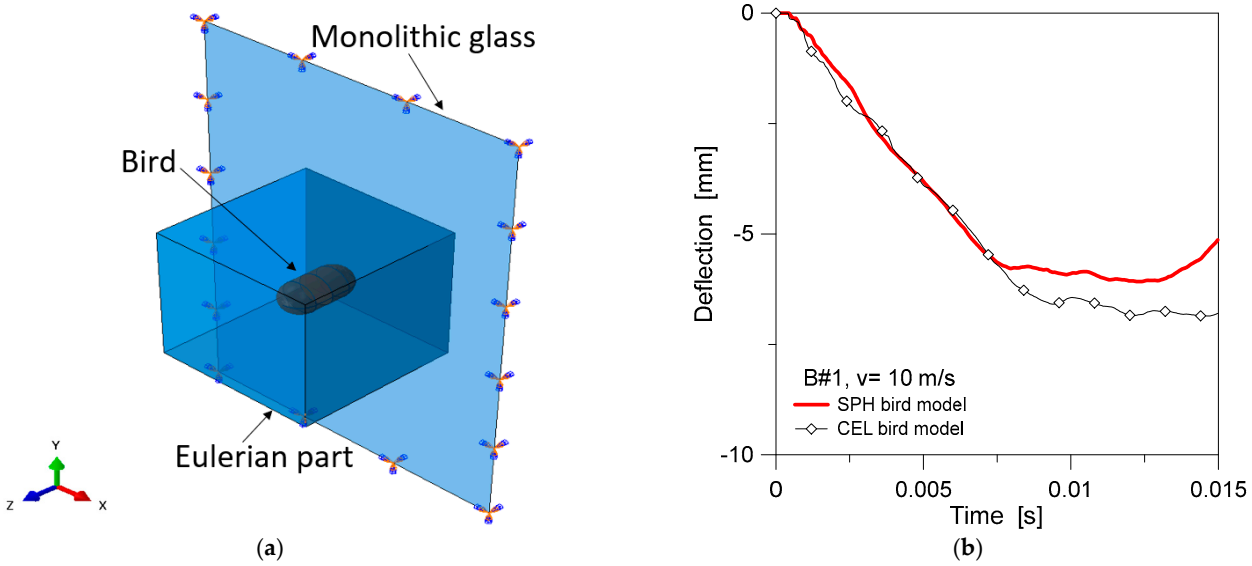

Figure 10. Preliminary bird-strike analyses: (**a**) monolithic glass panel under CEL bird collision (axonometric view); (**b**) comparison of measured deflection at the center of glass (ABAQUS/Explicit).

4. Parametric SPH–FE Numerical Analysis

Through the parametric SPH–FE numerical investigation, for a given $B \times H$ monolithic glass panel (as in Figure 11a), the attention was given to different locations for target points, as well as to the analysis of corresponding performance indicators/mechanical effects in glass, as a function of some basic modification in impact conditions (mass, size, and velocity). Overall, the bird-strike effect on a glass window can, in fact, be roughly schematized as a 2DOF system, like that in Figure 11b, where the reference impactor has an assigned velocity, mass, and stiffness. Accordingly, the target glass window reacts with a given stiffness and mass, while damping contributions can be generally neglected. Especially in the initial time instants of impact response, the reaction stiffness of the target panel is a rather local parameter that is affected by the bending stiffness, effect of boundaries, etc. Such a mechanical description is also in line with other impact conditions for glass windows and facades, but it requires major efforts for the calibration of input parameters [22].

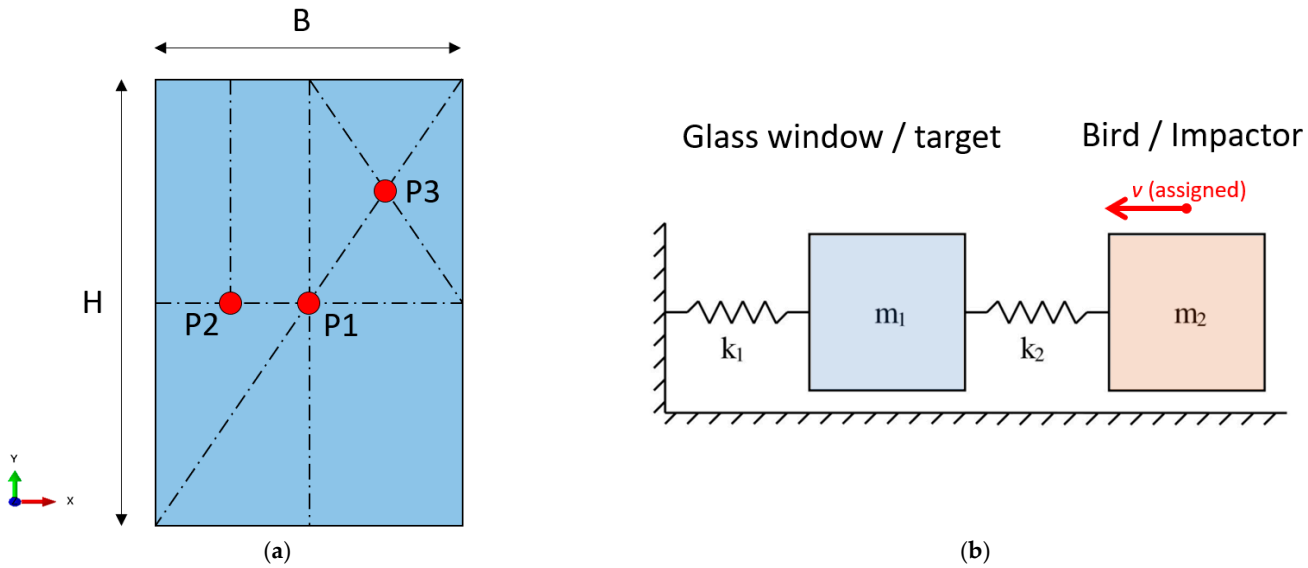

Figure 11. Schematic representation of (**a**) selected target points on glass (front view) and (**b**) 2DOF schematization for undamped glass window under bird-strike.

For the present study, the analysis of the glass side was focused on qualitative and quantitative performance assessment, e.g., the occurrence (if any) of cracks and the amount/extension of fractured glass panel compared to the original, intact size, or any kind of preliminary damage initiation.

To this aim, the examined configurations were characterized with a performance indicator herein defined to express the expected "damage severity" and its extension under the imposed bird collisions, so as to detect and quantify "major" collapses, "minor" damage, or even elastic behaviors. For fractured glass panels (i.e., with damage variable $D = 1$ from Section 3.2), such an assumption consisted of the quantification of eroded elements (calculated in terms of total volume of removed shell elements, V_f), compared to original window geometry (with uncracked volume $V_0 = B \times H \times t$). For impact scenarios characterized by limited/minor damage propagation in glass (i.e., $0 < D < 1$ and no element removal), the quantification of damage severity was expressed by measuring the total surface of elements with damage initiation (A_{dam}, that is the total surface of shell elements with $D > 0$), and the original intact surface $A_0 = B \times H$. The herein called normalized damage severity ratio was hence calculated as follows:

$$R_f = max\left(\frac{V_f}{V_0}; \frac{A_{dam}}{A_0}\right) \quad (6)$$

The so-calculated parameter ($0 \leq R_f \leq 1$ its range) was measured for all the examined configurations. According to Equation (6), $R_f = 0$ means no cracks opening or preliminary damage in glass (i.e., $D = 0$) and, thus, a fully elastic response of the panel under bird-strike. At the same time, R_f tending to 1 denotes a severe damage with glass fracture, collapse, and possible shards scattered against building occupants.

Overall, three different size/mass parameters were taken into account for the impactor ($M_1 = 1.81$ kg, $M_2 = 0.7$ kg, and $M_3 = 0.35$ kg). The corresponding velocity was explored in the range suggested by the literature documents (i.e., Table 1). Moreover, at least three different target points were taken into account, as in Figure 11 (up to 20 m/s for impactor B#1, and up to 40 m/s for impactor B#3). As a comparative parameter, the corresponding impact energy from Equation (1) was taken into account.

4.1. Impact Response

The typical impact response of a traditional glass panel is summarized in Figure 12 ($t = 6$ and B#1 for the P1 target in the example, with $v = 10$ m/s), in the form of deflection at the center and stress distribution at the center (on both the unexposed/compressed and exposed/tensioned sides of the monolithic section), with qualitative distribution of stress components at selected time instants (exposed/tensioned side). It is worth noting that the quantitative results, as shown in Figure 12, were taken into account as traditional performance indicators for the response of all the examined glass windows under localized impact scenarios, but a primary role was assigned to the damage-severity parameter, R_f, from Equation (6). In this manner, the expected dynamic behavior (and possible risk for people) was equally compared for windows with elastic response, or minor damage or even global collapse.

According to Figure 12, it can be seen that, as far as the window panel is able to resist against input pressure, stress peaks rapidly increase in the center but are characterized by fast propagation toward the region of restraints. As such, the stiffer the window/restraint is, the more attention should be paid to both the local and global performance analysis (i.e., to ensure possible risk of failure in the region of restraints).

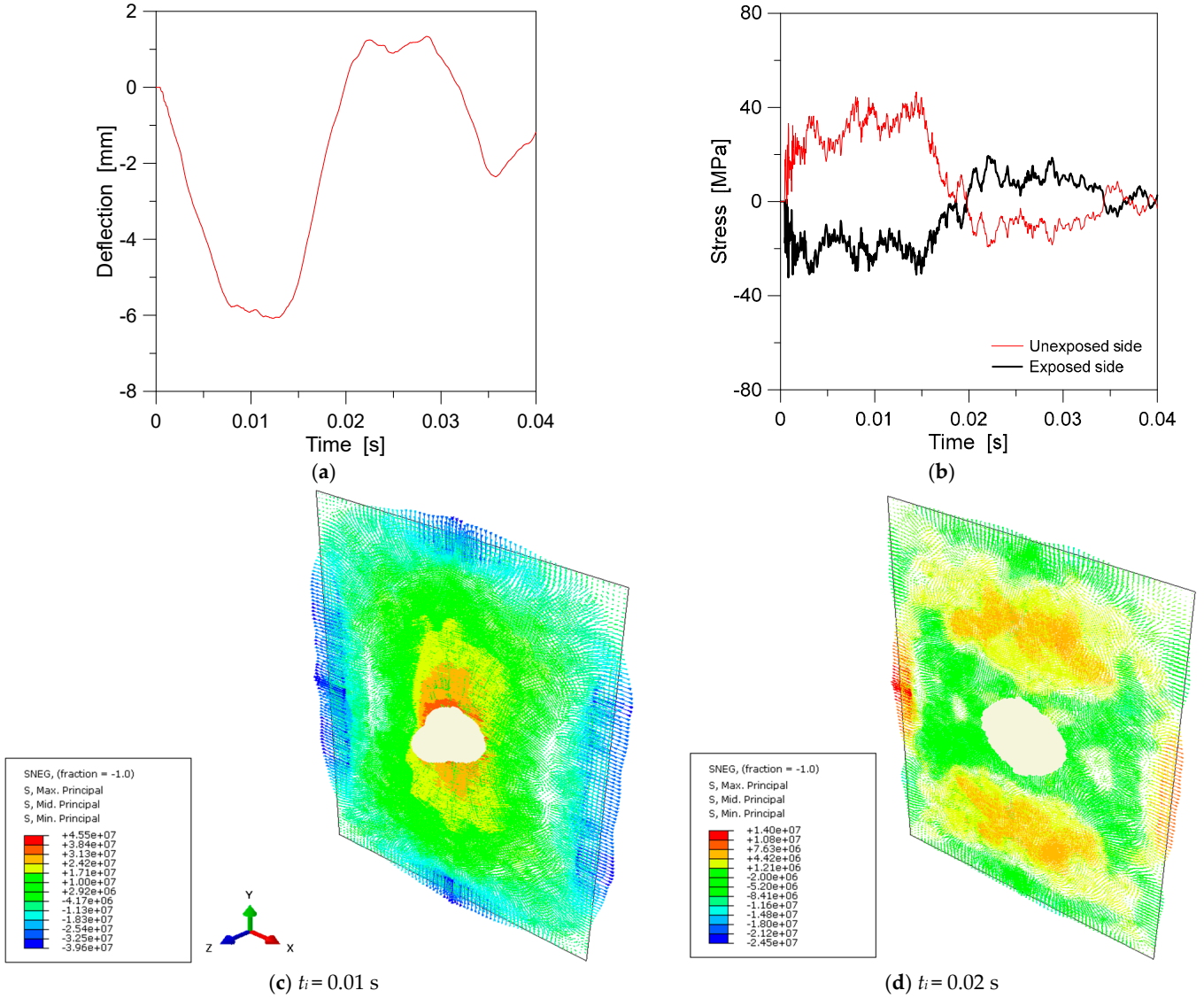

Figure 12. Example of bird-strike analysis: (**a**) deflection at the center of glass, (**b**) maximum stresses at the center of glass, and (**c**,**d**) stress distribution (legend values in Pa) at selected time instants (ABAQUS/Explicit). Example for t = 6 mm thick glass, B#1 impactor at the center (v = 10 m/s of impact speed).

4.2. Failure Mechanism

The failure mechanism for the examined glass panels was found to be dominated by material brittleness and limited tensile strength (Figure 13). At the same time, however, a strong correlation was observed between the global bending stiffness of the glass panel (as a function of it thickness t and size $B \times H$), the local stiffness (as a function of impact point), and the mass M/speed (v) of bird impactor.

Overall, the typical impact response lasted for a maximum of t_i = 40 ms (with an average of t_i = 18 m/s), depending on the loading setup. In Figure 13a, an example of sequential damage can be seen for one of the investigated panels (H = 1.5 m, B = 1 m, t = 4 mm, with B#1 in P1 at an imposed speed of 10 m/s, corresponding to ≈90 J of impact energy). It can be noted (for the examined setup) that the glass panel first reacts elastically, and the bird body undertakes minor deformations in the impact region. Moreover, as far as the tensile strength of glass is first exceeded, damage initiation begins with the opening of cracks and progressive propagation of fragments.

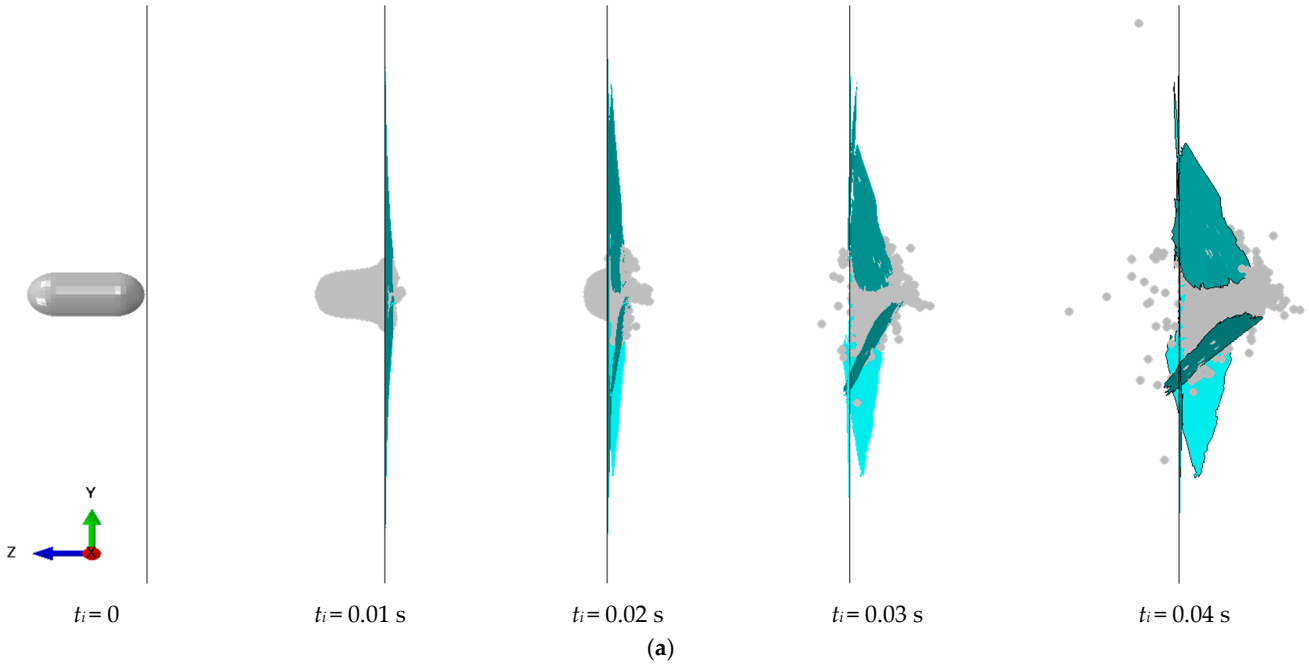

(**a**)

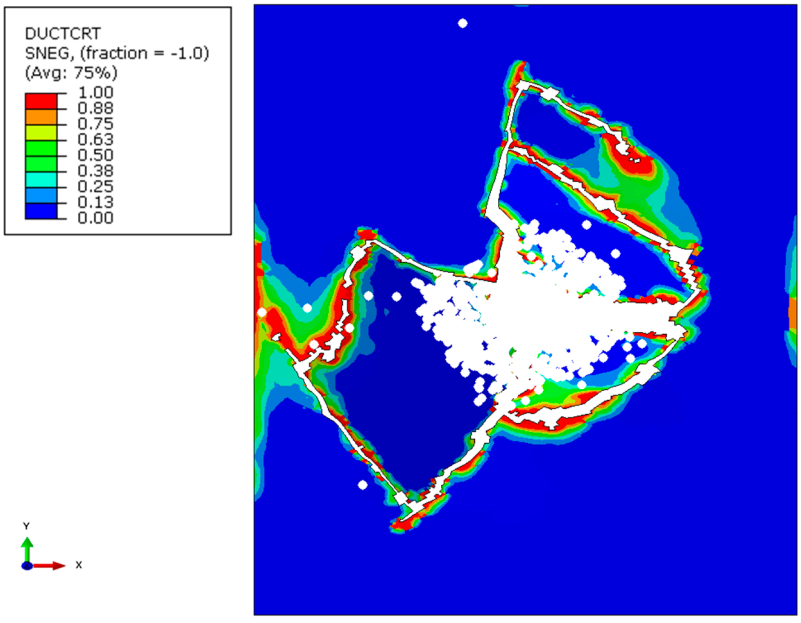

(**b**) t_i = 0.04 s

Figure 13. Example of failure mechanism for glass panel under B#1 impactor (v = 10 m/s): (**a**) sequential side view and (**b**) front view with damage distribution (ABAQUS/Explicit).

Figure 13b shows the same failure configuration from the front view (t_i = 0.04 s), with evidence of glass fragmentation and damage parameter. Maximum values denote the loss of bearing capacity (D = 1). It is interesting to note, as expected, that the fracture of the glass panel originates in the central/target region, but also propagates toward the edge restraints. Whilst the bird-strike is hence recognized as a local event, in this sense, the global dynamic response and the expected damage phenomena for a given system should be properly explored and possibly mitigated.

From the parametric analysis and Equation (6), in terms of fractured portion of panel, the damage trend in Figure 14 was found. Numerical results are proposed for different glass thicknesses, imposed velocity, and, thus, impact energy, but at a fixed impact point (P1). Overall, a rather scattered trend can be noted for the calculated R_f parameter as a function

of input energy. This effect can be justified because of the sensitivity of the impactor and glass material to the strain rate, and thus in the qualitatively different failure mechanisms that can be expected for a given panel. Since the impact energy is rather small (less than ≈100 J, in the present study), rather null damage can be generally expected, given that local stress peaks can hardly exceed the reference tensile strength of glass. For this reason, the R_f values in Figure 14 are close to zero (no damage).

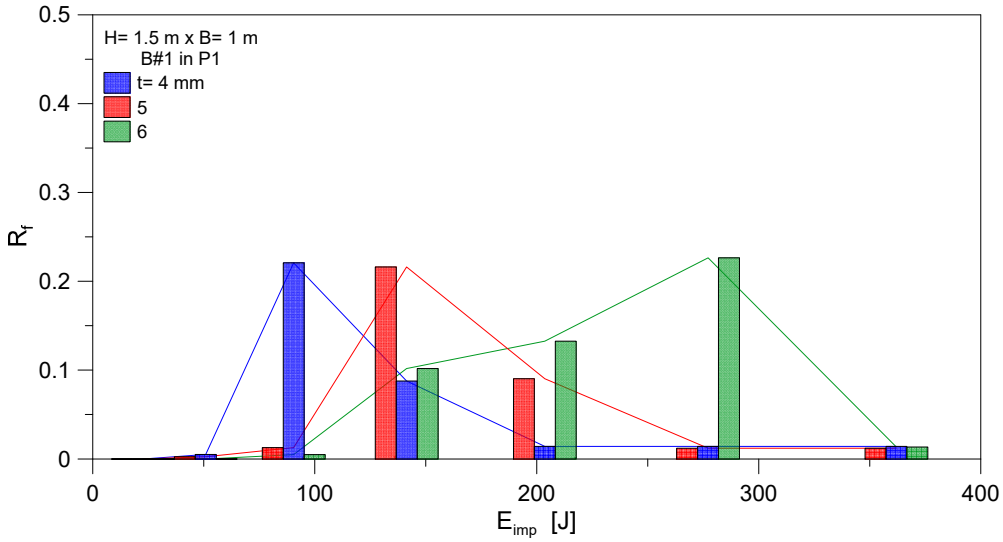

Figure 14. Calculated damage severity for a glass panel under B#1 impactor, as a function of impact energy, by changing glass thickness (ABAQUS/Explicit).

Increasing the imposed speed and impact energy evolves in Figure 14 to severe damage of glass, given that the material strength is exceeded, and several cracks can propagate, as in Figure 13. At this stage, however, the global and local stiffnesses of the panel, as well as the stiffness of impactor, can evolve in markedly different behaviors. For this reason, the damage-trend peak in Figure 14 is achieved, when changing glass thickness, for different impact energies/configurations. Accordingly, the thick glass panel (t = 6 mm) suffers the more severe damage distribution when compared to the initial configuration. This suggests that the more flexible the target panel is, the less severe/extended the expected damage (for low–medium-impact energies). When the impact energy is relatively high (and this represents the limit condition of v = 20 m/s for B#1 impactor type), the damage trend in Figure 14 tends again to zero. However, such a kind of finding has no correlation with initial chart data (no damage); instead, it represents a rather localized failure of glass, due to the relatively high speed of impactor (herein called "shot-like" failure).

A qualitative comparison of different breakage patterns can be seen in Figure 15 (for the t = 6 mm thick panel), where the bird impactor (SPH model) is detected by white elements. In Figure 15a, rather null damage can be measured in glass (i.e., no visible cracks), with a rather linear elastic response and minor damage/initiation only (i.e., mechanical degradation of material properties in post-elastic stage). In Figure 15b, major cracks propagate from the center and also affect the region of restraints (severe damage). In Figure 15c, finally, an example of "shot-like" fracture pattern is proposed.

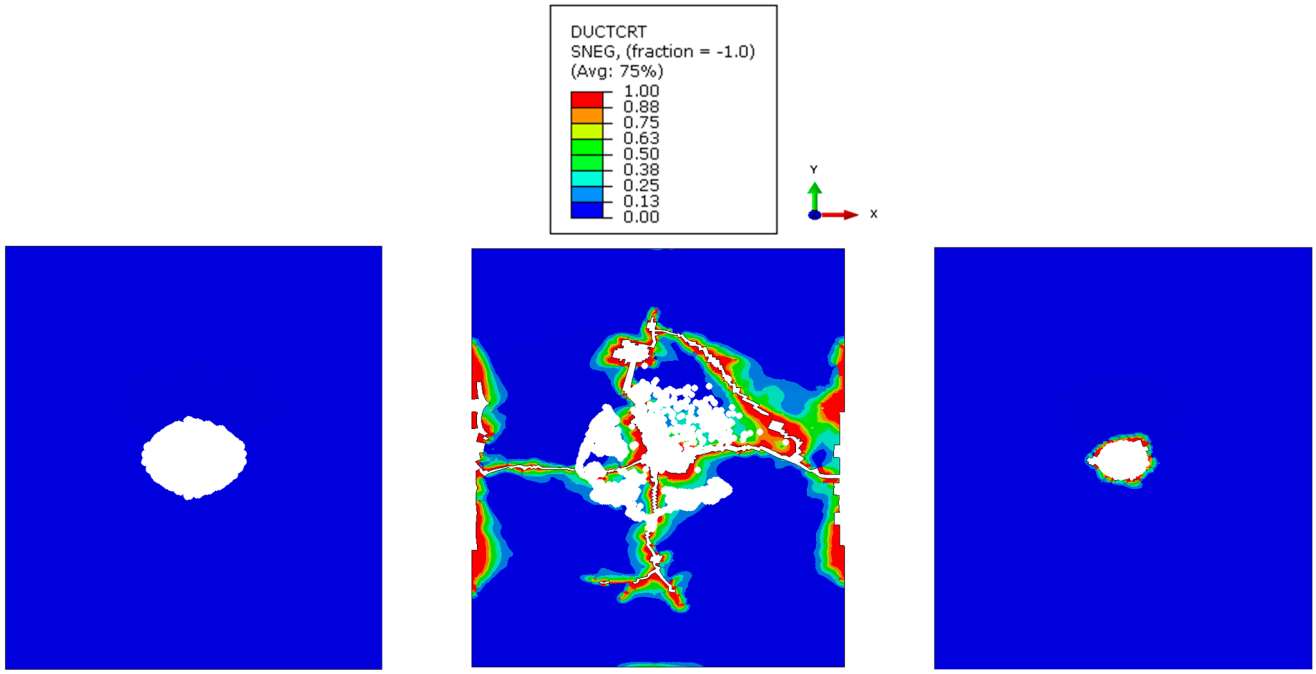

(**a**) Minor/initiation (v = 10 m/s) (**b**) Severe (v = 15 m/s) (**c**) Shot-like (v = 20 m/s)

Figure 15. Qualitative comparison of failure mechanisms for a t = 6 mm thick glass panel under B#1 impactor (front view, ABAQUS/Explicit).

4.3. Impactor Size

The analysis was focused on conducting a vulnerability assessment of the glass panel under equivalent impact energy from Equation (1), but resulting from impactors B#1, B#2, and B#3, with different imposed speeds (Figure 16).

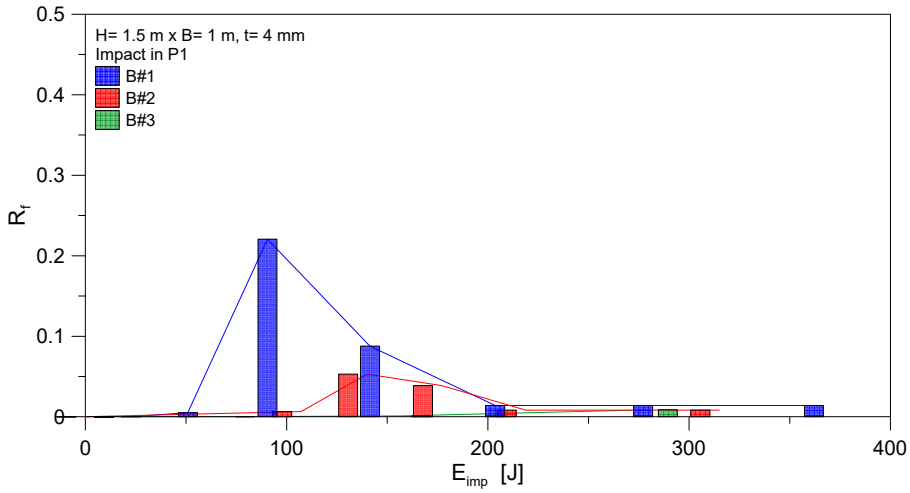

Figure 16. Calculated damage severity for a glass panel under B#1, B#2, or B#3 impactors, as a function of impact energy (ABAQUS/Explicit).

As far as the B#1 impactor is replaced by B#2 (less than half size), damage looks more localized and still pronounced above ≈100 J of impact energy, but with slightly reduced severity and a rather null effect on lateral boundaries. In the case of the B#3 impactor, this stress and damage concentration is even more pronounced, and it is rather null for impact energy below ≈250 J. As also qualitatively expected, the size of the impactor compared to the geometrical and mechanical properties of the target windows is also a relevant influencing parameter. From the comparative analysis in Figure 16, it can be observed

that failure risk for ordinary glass elements to small-size bird impact (like B#3, in the present study) is limited and may be critical for a relatively high impact speed/energy only (out of conventional speed ranges). In the case of a medium-size bird impact (like B#2, in the present study), monolithic glass panes of typical use for ordinary windows can be expected to be subjected to moderate damage, even under a relatively small impact energy/limited speed. This means that mitigation techniques should possibly be taken into account. On the other side, damage evolution and distribution were found to be rather localized and to result in a relatively small number of possible shards. For monolithic glass windows subjected by a possible large-size B#1 type impactor, finally, the analysis of results in Figure 16 confirms that severe damage can be expected, and the most severe conditions are characterized by a relatively low impact speed (about ≈100 J of impact energy), resulting in a large number of glass fragments, rather than a high-speed impact (with shot-like failure mechanism).

4.4. Target Point

Successively, the effects due to a given impactor with assigned speed for a target glass panel and different impact points were explored. The influence of restraints, as well as the bending stiffness of target panel, is notoriously associated with a multitude of possible dynamic phenomena (and thus possible damage scenarios). This is in line with standardized protocols for testing the vulnerability of facades under soft-body/human impact [22], as well as with the general mechanical model of Figure 11b.

Figure 17a, for example, shows the out-of-plane displacement in time, with evidence of typical behaviors. For the examined impact conditions, it can be noted that maximum deflection effects can be rationally expected for impact in the center of window (P1 control point), under a fixed impact energy. This happens when the target point coincides with P1 but maximum deflection peaks are relatively high also for the panel subjected to other impacts. Such a finding can be noted by comparing the displacement-time histories of P1 and P3 control points when the target point coincides with P3. It can be noted that the maximum bending deformation is measured in P3 (target) at around 3 mm, and that is less than the 50% part of the P1 target scenario. This is slightly higher than P1 displacement due to the P3 target (2.6 mm), and again less than the 50% part of the P1 displacement under the P1 target.

Furthermore, local stress peaks should also be carefully addressed for target points that are close to window restraints and, thus, are possibly affected by local stiffness phenomena. The typical trend of maximum principal stresses in glass is, in fact, shown in Figure 17b for P1 and P3 control points. In P1, stress trends are shown both under the P1 target and P3 target of B#1. In the first case, the comparative analysis of selected stress plots shows that maximum peaks in P1 are recorded for about ≈0.02 s of the initial bending response. When the target point is moved to P3, stress evolutions in P3 are characterized by a relatively shorter time interval of maximum peaks (less than 0.01 s) compared to P1. This results also from the contact of the bird and its interaction with the progressive bending deformation of the panel. In this regard, it is worth noting that absolute stress peaks in P1 (with P1 target) and P3 (with P3 target) in Figure 17b are quantitatively similar, even with a different evolution of deflections (Figure 17a). When P1 stresses are monitored for impact configurations with different target points (like P3, for example), stress peaks are relatively small. Finally, Figure 17c gives evidence of the progressive bending deformation of the examined panel (P3 target point), where the selected contour plots emphasize the combination of both a local deformation (in the region of impact) and an unsymmetric global bending deformation of the panel, with a consequent distribution of deflections and stress peaks in time.

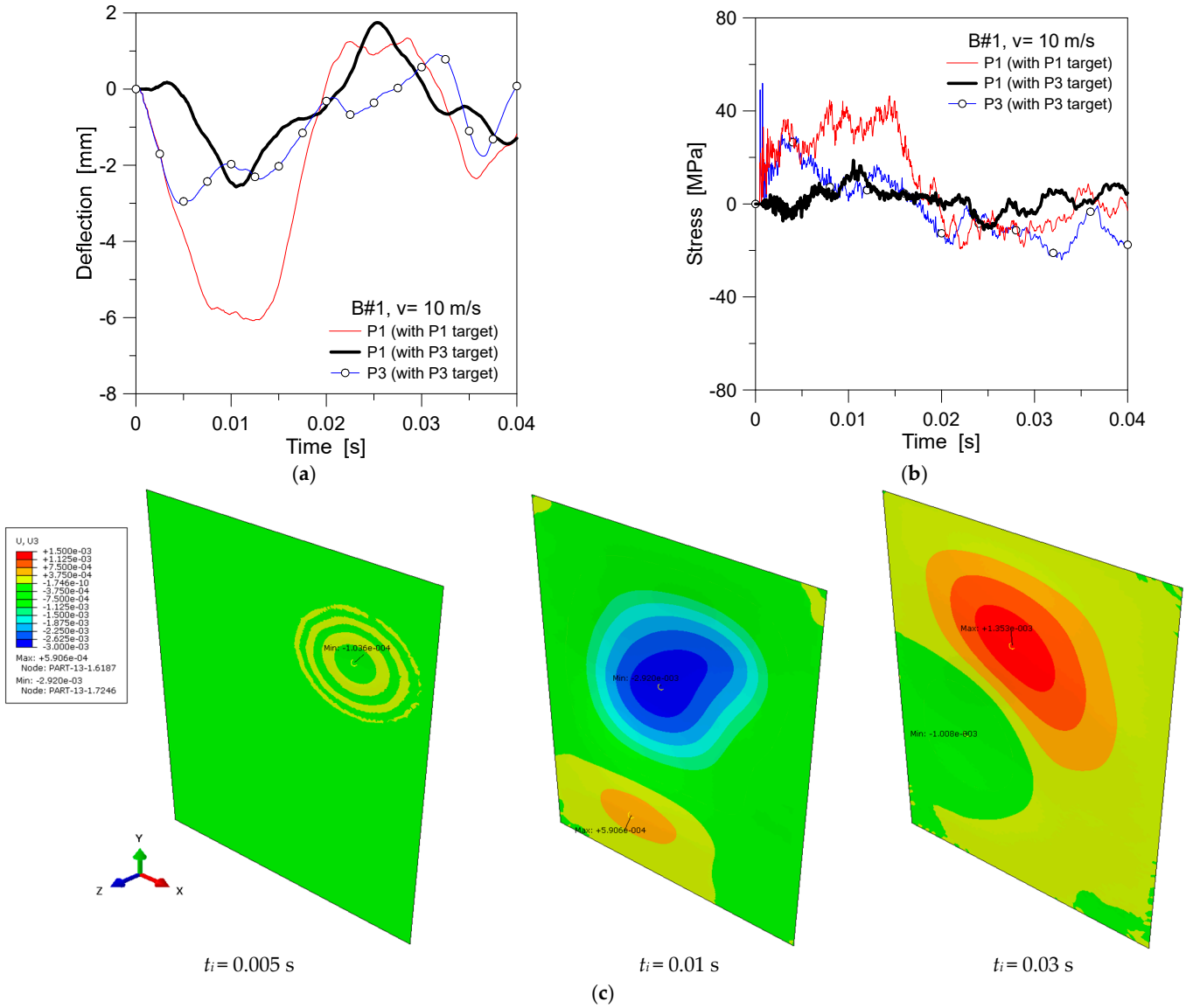

Figure 17. Example of bird-strike analysis for a given glass panel under B#1 impact (v = 10 m/s) in different target points (P1 or P3): time history in P1 in terms of (**a**) deflection and (**b**) maximum stresses, with (**c**) contour plot of out-of-plane deformations for P3 target point (with scale factor ×10 on deformations and legend in m, ABAQUS/Explicit).

5. Empirical Approach for Vulnerability and Capacity Check

5.1. Operational Steps of Simplified Procedure

A simplified graphical approach was developed on the basis of SPH–FE numerical observations and some analytical considerations. Such an approach could represent a first insight into the situation and support a rapid vulnerability analysis, especially for existing ordinary glass elements where load-bearing capacity could be not required but safety levels against possible accidental failure could be, in any case, required. For the present procedure, the conventional B#1 is taken into account as a reference. Furthermore, a panel size with $H = 1.5 \times B = 1$ m is considered to be a conventional window.

To this aim, the detailed study of SPH–FE results was focused on the analysis of stress peaks and damage initiation/evolution as a function of impact conditions. The attention was given to the definition of a threshold configuration that could correlate the dynamic parameters of the ordinary glass panel with the impactor features. As such, three reference conditions were detected and are defined as follows:

- First occurrence of minor damage/damage initiation (noted as D1 damage level), without visible cracks in glass, but with measurable degradation;
- First occurrence of severe damage (D2);
- First occurrence of shot-like damage (D3).

The Basic assumptions and limitations of the simplified procedure are as follows:

- Monolithic glass panels only are taken into account;
- Rigid linear restraints are considered at the edges of glass, and any kind of possible damage in boundaries is disregarded;
- The maximum size of the bird impactor is set at 1.81 kg and conventional dimensions are like those in Figure 6 and Reference [2], while reference (and realistic) impact-speed values should be derived for the species of interest (like in Table 1 of the present investigation).

Thus, careful consideration should be paid for different mechanical configurations (i.e., cross-section of glass, or even presence of weak/flexible boundaries or mechanical/adhesive point-fixings of typical use, especially for new glass components, etc.).

Once the vulnerability has to be addressed for an existing window/envelope, the minimum D1 damage represents the threshold condition to satisfy the safety check.

For the B#1 impactor, the threshold impact-speed values are reported in Figure 18a, based on the postprocessing analysis of the SPH–FE numerical results. For a given panel with frequency f_1, each plot denotes the possible impact conditions with the minimum speed leading to a specific damage scenario (D1, D2, or D3). It must be noted that dots are reported as calculated from the SPH–FE numerical analyses. On the other side, the proposed threshold curves are voluntarily presented with a linear trend in order to simplify the analytical calculation and, at the same time, preserve a certain safety margin, as compared to more accurate SPH–FE numerical outcomes and even more complex real scenarios.

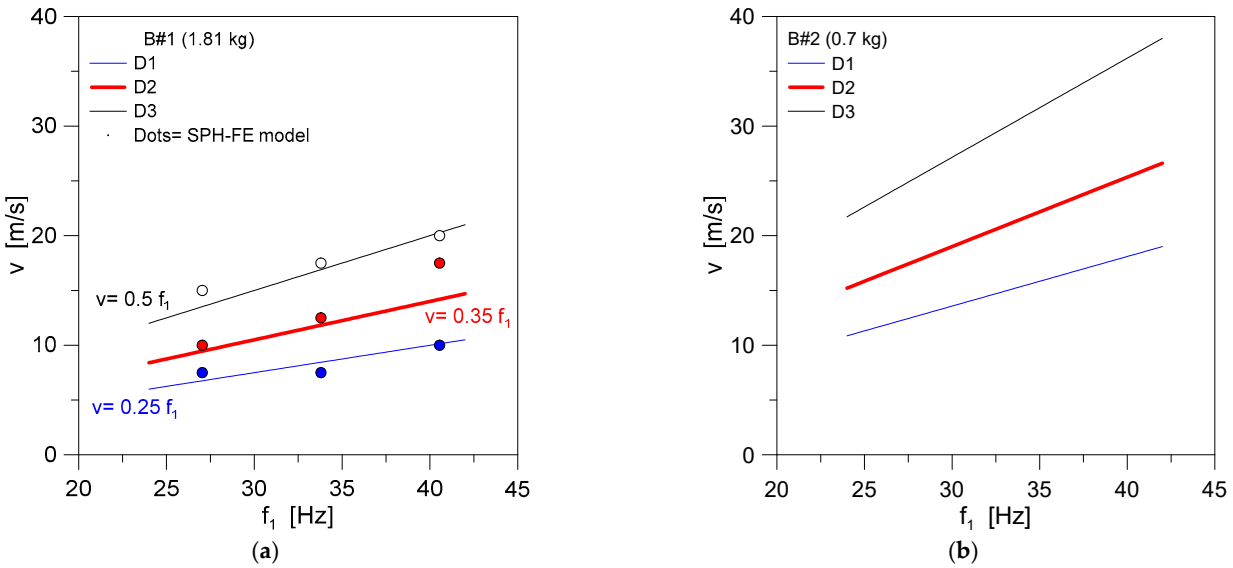

Figure 18. Calculated correlation of damage levels (D1, D2, and D3) as a function of vibration frequency and imposed impact speed for a glass panel under (**a**) B#1 or (**b**) B#2 impactors (ABAQUS/Explicit).

As far as the impactor changes, see Figure 18b for B#2 impactor, a rather proportional correlation was found with B#1 results, as a function of mass ratio. This suggests that a mass ratio correlation can be possibly derived for simplified estimates.

In terms of impact energy, by taking B#1 impactor as a reference, for a general impactor size (B#n impactor, with mass $M_{B\#n}$ and diameter from Equation (4)), the corresponding

impact condition can be in fact calculated as in Figure 19, that is based on threshold velocity values in Figure 18a, herein denoted as $v_{ref,B\#1}$, and the mass ratio R_M:

$$E_{imp,B\#n} = \frac{1}{2}\left(v_{ref,B\#1}\right)^2 R_M \tag{7}$$

and

$$R_M = \frac{M_{ref,B\#1}}{M_{B\#n}} \tag{8}$$

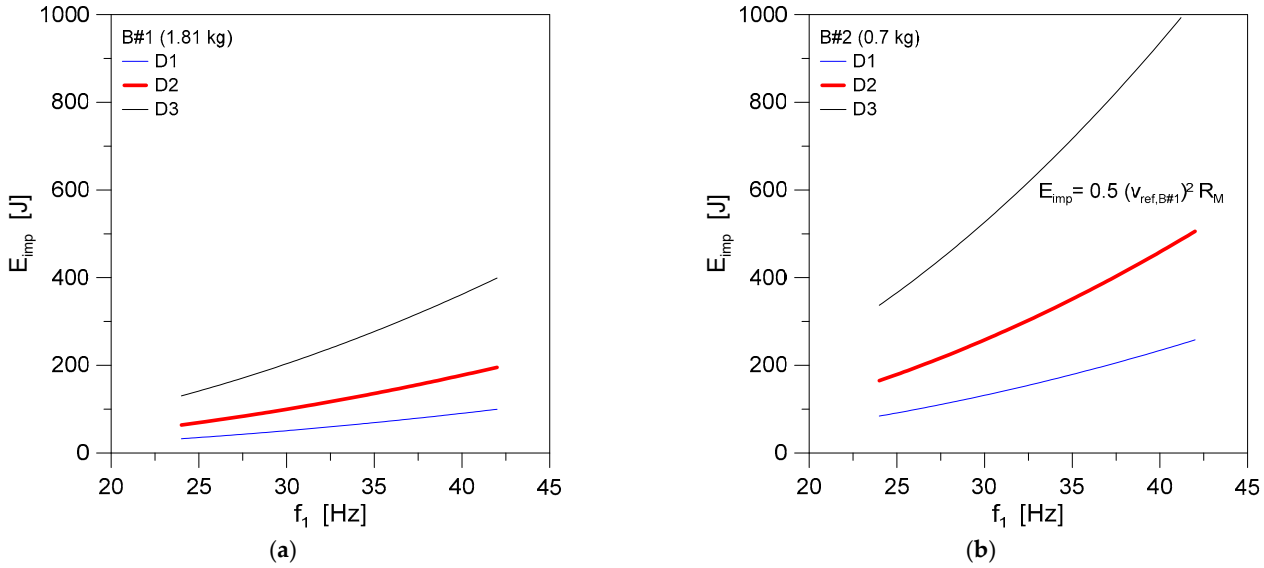

Figure 19. Calculated correlation of damage levels (D1, D2, and D3) as a function of vibration frequency and imposed impact energy for a glass panel under (**a**) B#1 or (**b**) B#2 impactors (ABAQUS/Explicit).

The overall simplified empirical approach requires that the fundamental vibration frequency of the glass panel object of study, f_1, is first calculated or at least approximately estimated. Under the approximate assumption of continuous restraints along the edges (ideal boundary condition), this can be roughly analytically predicted as follows:

$$f_{n,m} = \frac{\pi}{2}\left[\left(\frac{n}{H}\right)^2 + \left(\frac{m}{B}\right)^2\right]\sqrt{\frac{D_b}{\gamma}} \tag{9}$$

with $n = 1$, $m = 1$ for the fundamental vibration mode, $H \times B$ the edge size, and D_b the bending stiffness of panel:

$$D_b = \frac{E_g t^3}{12(1-\nu^2)} \tag{10}$$

where γ is its mass per unit of surface.

In general, a linear modal analysis of the edge restrained panel could also be carried out with FEA and software support, to predict f_1.

It is worth noting that, once the f_1 is known, the vulnerability and capacity check against bird-strike could be derived for a general glass panel under bird collision, with major benefits on design from the use of such a practical tool. Limits of the presently developed simplified approach, however, are represented by the following:

- Shape of target glass panel (i.e., non-rectangular panes could suffer for additional sensitivity effects);
- Glass type (float annealed glass is only considered, disregarding any pre-stress contribution);

- Boundary conditions (linearly restraints are taken into account, disregarding other boundary configurations of typical use for glass panels);
- Fixed examined range of bird collision parameters (as in Section 4), based on the case-study system described in Table 1;
- Maximum impact energy of 400 J, following the above point.

5.2. Application of Simplified Procedure to Full-Size Envelopes

For further assessment of the above vulnerability considerations, as well as for confirmation of small-scale outcomes previously discussed, the above SPH–FE modeling and empirical strategy was applied to a full-size glass envelope characterized by the presence of monolithic, thin glass panels (t = 5 mm in thickness) used to cover relatively wide surfaces. More precisely, the full-size calculation was inspired by the case-study system schematized in Figure 2, which was described in Reference [37], and subjected to in-field experimentally characterization in Reference [52].

Most importantly for dynamic behavior considerations, the full-size system is characterized by a fundamental vibration frequency f_1 = 6.58 Hz [52], and its dynamic behavior is dominated by the first vibration shape of its central portion of glass (H = 3.3 × B = 2.58 m in size), which works as a continuously restrained thin monolithic panel in out-of-plane bending. This response can be noted in Figure 20a, as obtained from a linear modal analysis of the envelope. For bird-strike analysis, a dedicated structural FE model was in fact described in ABAQUS/Explicit the form of shell monolithic elements reproducing the nominal geometry of glass panels and the supporting steel members of frame [52]. Rigidnodal boundaries were applied to frame members. This choice resulted in a total of ≈30,000 elements for the structural part and ≈170,000 DOFs. The 3D bird body for impact simulations was described with the SPH approach earlier described in Section 3. Similarly, material properties (for glass and bird) and solving strategies were kept as discussed in Section 3. As such, the typical SPH–FE numerical analysis consisted in a non-linear dynamic step with imposed impact speed for the assigned bird impactor. This impact step was carried out after a preliminary linear modal analysis to capture the fundamental vibration frequencies and shapes of the system.

In terms of impact performance, the full-size steel–glass envelope was found still characterized by dynamic response governed by out-of-plane bending deformation of the central panel exposed to strike. The principal stress distribution and evolution in glass was also found maximum localized in the region of target point and successively propagating to the other parts of the steel–glass composite system (see an example in Figure 20b).

In this context, a first set of non-linear dynamic simulations and damage severity estimated was parametrically carried out. Figure 20c presents the expected R_f damage amount for the same steel–glass system under B#1 impactor (target point at the center of panel). Input values of histogram chart were numerically derived based on Equation (6). The maximum impact energy for the parametric configurations in Figure 20c was set in a top value of 400 J, due to realistic mass and velocity input values for the examined scenarios. In this sense, higher impact energies for the same B#1 mass would necessarily require an impact speed which is out of ranges for conventional values as in Table 1. It can be seen that the calculated R_f parameter progressively increases from zero when the impact energy is in the range of ≈141 J (with R_f = 0.09, no cracks).

Under soft-body impact, the impactor features but also the target system features (especially their equivalent dynamic parameters) should be properly taken into account, as in the form of a mechanical 2DOF system (see for example [22]).

For threshold damage conditions as in Figure 19a, in this regard, the size effect of glass panel must be also taken into account, and its aspect ratio compared to the reference window panel from Figure 4. Based on the predicted effects under B#1 impactor, more precisely, this size effect can be approximately taken into account as follows:

$$v_{size} = v_{ref,B\#1} R_{size} \tag{11}$$

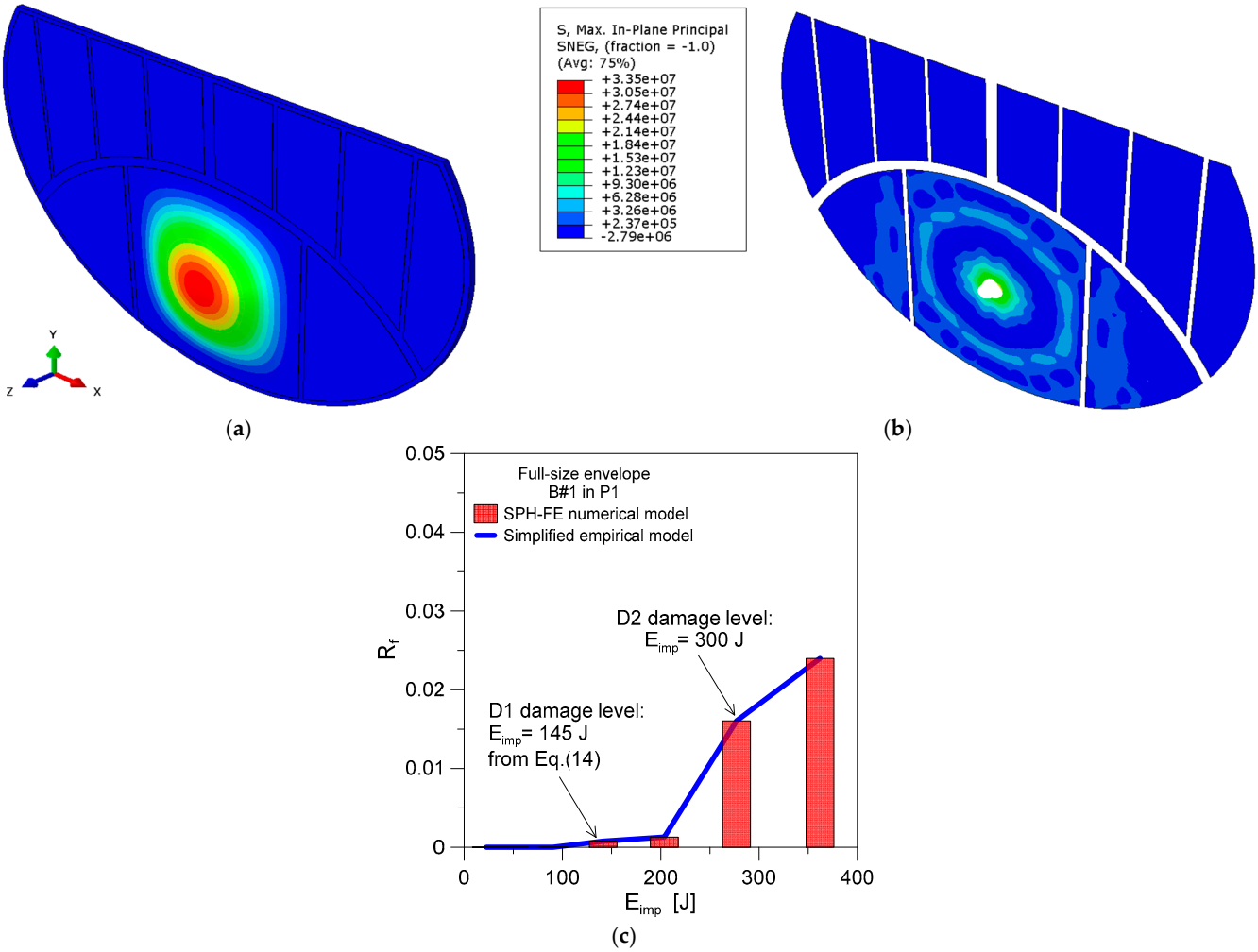

Figure 20. Round-shaped steel–glass facade: (**a**) fundamental vibration shape (linear modal analysis; mesh hidden from view, extruded axonometry); (**b**) example of stress distribution under B#1 impactor (v = 10 m/s, legend values in Pa; mesh and steel frame hidden) and (**c**) calculated damage severity (SPH–FE values based on Equation (6)) under B#1 impactor at the center of glass.

Moreover, with $v_{ref,B\#1}$ from Figure 19a, we have the following:

$$R_{size} = \frac{M_{size}}{M_{ref}} \tag{12}$$

where M_{ref} (in kg) is the mass of reference window in Figure 19 (≈15 kg), while M_{size} is the mass (in kg) of the general one (for the present study, the target glass system in Figure 20). Assuming that f_1 = 6.58 Hz for the full-size panel, the minimum speed for minor damage/possible initiation of degradation risk (D1 level) is given by the following:

$$v_{size} = v_{ref,B\#1} R_{size} \approx (0.25 f_1) \frac{116}{15} = 12.6 \text{ m/s} \tag{13}$$

Thus, we have the following:

$$E_{imp,size} = \frac{1}{2} (v_{size})^2 M_1 \approx 145 \text{ J} \tag{14}$$

It is worth noting from Figure 20c that the impact condition for minimum damage initiation was numerically predicted under an imposed impact energy, and this—even under simplifications of the empirical procedure—is in close agreement with Equation (14).

A good correlation can be noted both for D1 and for D2 damage levels. Minor D1 damage is numerically expected in Figure 20c for an impact energy of ≈141.5 J, which has a scatter of 2.4% compared to Equation (14).

From a practical point of view, this means that a typical B#1 impactor type with impact velocity of ≈12.6 m/s or higher (according to Table 1) could manifest—for the investigated full-size steel–glass envelope—in minor damage initiation that should be properly taken into account to prevent possible risk for occupants and be mitigated with appropriate tools and techniques. Similarly, the simplified approach could be used for existing glass systems that are—especially in historic or monumental or old ordinary buildings—not specifically designed to resist accidental impact.

It is also worth to note in Figure 20c that the simplified analytical approach for the examined case-study system would result in a minimum impact speed of ≈18 m/s (corresponding to a minimum of ≈300 J of impact energy) to detect the threshold condition for the D2 damage level. It can be seen in Figure 20c that there was a moderate increase of the numerically calculated R_f values in the range of 300 J of imposed impact energy (≈278 J). Compared to D1, it must be noted that the calculated scatter for D2 limit is up to 7.8%, and, thus, further calibration would be required for the generalized use of the simplified approach. Moreover, this D2 condition is close to the maximum available speed for the examined impactor/bird type in Table 1 and, thus, less probable than D1. Finally, it should be noted that the D3 damage level would be analytically quantified with a minimum risk of occurrence for the examined case-study system. In fact, the simplified approach would result in a threshold velocity of ≈25.6 m/s (corresponding to ≈600 J of impact energy), which is largely above the range of practical interest of real collision scenarios.

In this sense, the attention will be spent on a further extended assessment and validation of the presently reported empirical calculation method, so as to include a wide set of geometrical and mechanical configurations of technical interest for building retrofit and mitigation in historic/existing constructions.

6. Conclusions

Especially in historic/old buildings, glass components and partitions are mostly characterized by monolithic glass sections which, in the past, have not been properly designed to sustain mechanical design loads, as it is nowadays required by standards for these load-bearing elements. This results in possible risk for occupants, due to limited resistance and capacity to accommodate even relatively low accidental design actions.

In this paper, based on inspiration from a full-size thin-glass-envelope case study built up in Italy in the 60s, a parametric numerical study was focused on the bird-strike impact performance of ordinary annealed monolithic glass panels of typical use in old buildings. More in detail, based on a coupled SPH–FE numerical modeling technique, various impact configurations were taken into account by changing the impactor size, mass, speed, and target point (up to 1.81 kg of bird mass, 40 m/s of collision speed and 400 J of corresponding impact energy). Attention was given to annealed monolithic glass panels with a thickness in the range of 4 to 6 mm. The local and global analysis of performance parameters for such relatively fragile building components was hence carried out to derive general indicators for residual capacity and vulnerability of these systems. In this regard, the postprocessing stage was focused on the definition of a damage severity parameter, so as to quantify and express the expected damage level (D1 to D3 levels in the present study) and its extension on a given glass panel, under a set of input parameters for bird collision (first of all, the impact energy).

Furthermore, the parametric SPH–FE numerical parametric study was used to derive simple analytical equations and normalized charts for a simplified empirical model, so as to obtain preliminary predictions for soft-body bird-strike effects on monolithic glass panels. As a case-study system, the simplified procedure was applied to an Italian case study of a historic steel–glass envelope, given that it is characterized by relatively thin monolithic glass thickness (5 mm only) for several meters of covered surface. The anal-

ysis of the SPH–FE numerical results from the nonlinear dynamic-impact simulations and preliminary analytical estimates from the simplified approach suggests rather good agreement and the potential of such a kind of procedure for performing a vulnerability analysis and mitigation planning in historic glass components. At the same time, further extended parametric studies are currently required to cover a multitude of geometrical and mechanical configurations of technical interest for building applications.

Author Contributions: C.B., conceptualization, methodology, software, validation, and writing—original draft preparation; M.V.S., investigation and writing—original draft preparation. All authors have read and agreed to the published version of the manuscript.

Funding: This research received no external funding.

Data Availability Statement: Data will be shared upon request.

Conflicts of Interest: The authors declare no conflict of interest.

References

1. Metz, I.C.; Ellerbroek, J.; Mühlhausen, T.; Kügler, D.; Hoekstra, J.M. Analysis of risk-based operational bird strike prevention. *Aerospace* **2021**, *8*, 32. [CrossRef]
2. Federal Aviation Administration, Dept. of Transportation. *Bird Strike Damage. Part 25 Airworthiness Standards: Transport Category Airplanes*; Sec. 25.631; Federal Aviation Administration: Washington, DC, USA, 2003.
3. Plassard, F.; Héreil, P.-L.; Joseph, P.; Mespoulet, J. Experimental and numerical study of a bird strike against a windshield. *EPJ Web Conf.* **2015**, *94*, 01051. [CrossRef]
4. Liu, J.; Li, Y.; Gao, X. Bird strike on a flat plate: Experiments and numerical simulations. *Int. J. Impact. Eng.* **2014**, *70*, 21–37. [CrossRef]
5. Airoldi, A.; Cacchione, B. Modelling of Impact Forces and Pressures in Lagrangian Bird Strike Analyses. *Int. J. Impact. Eng.* **2006**, *32*, 1651–1677. [CrossRef]
6. Smojver, I.; Ivančević, D. Numerical Simulation of Bird Strike Damage Prediction in Airplane Flap Structure. *Comp. Struct.* **2019**, *92*, 2016–2026. [CrossRef]
7. McCarthy, M.; Xiao, J.R.; McCarthy, C.; Kamoulakos, A.; Ramos, J.; Gallard, J.P.; Melito, V. Modeling of bird Strike on an Aircraft Wing Leading Edge Made from Fiber Metal Laminates—Part 1: Material Modeling. *Appl. Comp. Mater.* **2004**, *11*, 295–315. [CrossRef]
8. Goyal, V.K.; Huertas, C.A.; Vasko, T.J. Bird-strike modeling based on the Lagrangian formulation using LS-DYNA. *Am. Trans. Eng. Appl. Sci.* **2013**, *2*, 57–81.
9. Heimbs, S. Computational methods for bird strike simulations: A review. *Comput. Struct.* **2011**, *89*, 2093–2112. [CrossRef]
10. Smetankina, N.; Malykhina, A.; Merkulov, D. Simulating of Bird Strike on Aircraft Laminated Glazing. *MATEC Web Conf.* **2019**, *304*, 01010. [CrossRef]
11. Feldmann, M.; Kasper, R.; Abeln, B.; Cruz, P.; Belis, J.; Beyer, J. *Guidance for European Structural Design of Glass Components—Support to the Implementation, Harmonization and Further Development of the Eurocodes*; Report EUR 26439; Dimova, P., Feldmann, D., Eds.; Joint Research Centre–Institute for the Protection and Security of the Citizen: Ispra, Italy, 2014. [CrossRef]
12. Henriksen, T.; Hansen, S.O. Design of Glass for High, Short Duration Wind Loads. In Proceedings of the Challenging Glass 2–International Conference on the Architectural and Structural Application of Glass 2010, Delft, The Netherlands, 20–21 May 2010; Volume 2, pp. 627–637. [CrossRef]
13. Overend, M.; Zammit, K.; Hargreaves, D. Applications of computational wind engineering in the design of glass facades. *Proc. Glass Perform. Days* **2007**, *2007*, 444–448.
14. Pomaranzi, G.; Bistoni, O.; Schito, P.; Rosa, L.; Zasso, A. Wind effects on a permeable double skin façade—The ENI head office case study. *Fluids* **2011**, *6*, 415. [CrossRef]
15. Bedon, C.; Zhang, X.; Santos, F.; Honfi, D.; Kozłowski, M.; Arrigoni, M.; Figuli, L.; Lange, D. Performance of structural glass facades under extreme loads—Design methods, existing research, current issues and trends. *Constr. Build. Mater.* **2018**, *163*, 921–937. [CrossRef]
16. Casagrande, L.; Bonati, A.; Occhiuzzi, A.; Caterino, N.; Auricchio, F. Numerical investigation on the seismic dissipation of glazed curtain wall equipped on high-rise buildings. *Eng. Struct.* **2019**, *179*, 225–245. [CrossRef]
17. Sucuoğlu, H.; Vallabhan, C. Behaviour of window glass panels during earthquakes. *Eng. Struct.* **1997**, *19*, 685–694. [CrossRef]
18. Bedon, C.; Amadio, C.; Noè, S. Safety issues in the seismic design of secondary frameless glass structures. *Safety* **2019**, *5*, 80. [CrossRef]
19. Biolzi, L.; Bonati, A.; Cattaneo, S. Laminated Glass Cantilevered Plates under Static and Impact Loading. *Adv. Civ. Eng.* **2018**, *2018*, 7874618. [CrossRef]
20. Figuli, L.; Papan, D.; Papanova, Z.; Bedon, C. Experimental mechanical analysis of traditional in-service glass windows subjected to dynamic tests and hard body impact. *Smart Struct. Syst.* **2021**, *27*, 365. [CrossRef]

21. Schneider, J.; Schula, S. Simulating soft body impact on glass structures. *Proc. Inst. Civ. Eng. Struct. Build.* **2016**, *169*, 416–431. [CrossRef]
22. Bez, A.; Bedon, C.; Manara, G.; Amadio, C.; Lori, G. Calibrated Numerical Approach for the Dynamic Analysis of Glass Curtain Walls under Spheroconical Bag Impact. *Buildings* **2021**, *11*, 154. [CrossRef]
23. Deng, R.-B.; Jin, X.-L. Numerical simulation for blast analysis of insulating glass in a curtain wall. *Int. J. Comput. Meth. Eng. Sci. Mech.* **2010**, *11*, 162–171. [CrossRef]
24. Larcher, M.; Arrigoni, M.; Bedon, C.; van Doormaal, J.C.A.M.; Haberacker, C.; Hüsken, G.; Millon, O.; Saarenheimo, A.; Solomos, G.; Thamie, L.; et al. Design of Blast-Loaded Glazing Windows and Facades: A Review of Essential Requirements towards Standardization. *Adv. Civ. Eng.* **2016**, *2016*, 2604232. [CrossRef]
25. Pelfrene, J.; Kuntsche, J.; Van Dam, S.; Van Paepegem, W.; Schneider, J. Critical assessment of the post-breakage performance of blast loaded laminated glazing: Experiments and simulations. *Int. J. Imp. Eng.* **2016**, *88*, 61–71. [CrossRef]
26. Larcher, M.; Solomos, G.; Casadei, F.; Gebbeken, N. Experimental and numerical investigations of laminated glass subjected to blast loading. *Int. J. Imp. Eng.* **2012**, *39*, 42–45. [CrossRef]
27. Bedon, C.; Amadio, C. Numerical assessment of vibration control systems for multi-hazard design and mitigation of glass curtain walls. *J. Build. Eng.* **2018**, *15*, 1–13. [CrossRef]
28. Zhang, X.; Meng, Q.; Bedon, C.; Sielicki, P.W. Strengthening of Laminated Glass Windows against Windborne Debris Impact. *Int. J. Struct. Glass Adv. Mater. Res.* **2020**, *4*, 209–224. [CrossRef]
29. Haldimann, M.; Luible, A.; Overend, M. *Structural Use of Glass*; IABSE: Zurich, Switzerland, 2008.
30. *CNR-DT 210/2013*; Istruzioni per la Progettazione, L'esecuzione ed il Controllo di Costruzioni con Elementi Strutturali di Vetro; Guide for the Design, Construction and Control of Buildings with Structural Glass Elements. National Research Council of Italy (CNR): Roma, Italy, 2013.
31. *EN 572–2:2004*; Glass in buildings—Basic soda lime silicate glass products. CEN: Brussels, Belgium, 2004.
32. American Bird Conservancy. Bird-Friendly Building Design. 2015. Available online: https://abcbirds.org/wp-content/uploads/2015/05/Bird-friendly-Building-Guide_2015.pdf (accessed on 27 August 2022).
33. Goyal, V.K.; Huertas, C.A.; Vasko, T.J. Smooth particle hydrodynamic approach for bird-strike analysis using LS-DYNA. *Am. Trans. Eng. Appl. Sci.* **2013**, *2*, 83–107.
34. Simulia. *Abaqus Computer Software*; Simulia: Providence, RI, USA, 2021.
35. *CEN EN 12600:2002*; Glass in Building—Pendulum Test—Impact Test Method and Classification for Flat Glass. Beuth: Berlin, Germany, 2002.
36. *DIN 18008-4*; Glas im Bauwesen—Bemessungs-und Konstruktionsregeln—Teil 4: Zusatzanforderungen an absturzsichernde Verglasungen. Beuth: Berlin, Germany, 2013.
37. Santi, M.V.; Frangipane, A. Documenting the Factory-Town of Torviscosa (NE Italy): 1938–2020. In Proceedings of the Inheritable Resilience: Sharing Values of Global Modernities—16th International Docomomo Conference, Tokyo, Japan, 10–14 September 2021; p. 172877.
38. *Phasianus colchicus*, Avibase—The World Bird Database. Available online: https://avibase.bsc-eoc.org/species.jsp?lang=EN&avibaseid=4B9EEF568857FB51 (accessed on 7 October 2022).
39. *Columba livia*. Avibase—The World Bird Database. Available online: https://avibase.bsc-eoc.org/species.jsp?lang=EN&avibaseid=BBA263C235B15B88 (accessed on 7 October 2022).
40. Lavoie, M.A.; Gakwaya, A.; Nejad Ensan, M.; Zimcik, D.G. Validation of Available Approaches for Numerical Bird Strike Modeling Tools. *Int. Rev. Mech. Eng.* **2007**, *1*, 380–389.
41. Lavoie, M.; Gakwaya, A.; Ensan, M.N.; Zimcik, D.; Nandlall, D. Bird's substitute tests results and evaluation of available numerical methods. *Int. J. Imp. Eng.* **2009**, *36*, 1276–1287. [CrossRef]
42. Guida, M.; Marulo, F.; Meo, M.; Grimaldi, A.; Olivares, G. SPH—Lagrangian study of bird impact on leading edge wing. *Comp. Struct.* **2011**, *93*, 1060–1071. [CrossRef]
43. Yan, J.; Zhang, C.; Huo, S.; Chai, X.; Liu, Z.; Yan, K. Experimental and numerical simulation of bird-strike performance of lattice-material-infilled curved plate. *Chin. J. Aeron.* **2021**, *34*, 245–257. [CrossRef]
44. Zhou, Y.; Sun, Y.; Huang, T. Huang. SPH-FEM Design of Laminated Plies under Bird-Strike Impact. *Aerospace* **2019**, *6*, 112. [CrossRef]
45. Riccio, A.; Cristiano, R.; Saputo, S.; Sellitto, A. Numerical methodologies for simulating bird-strike on composite wings. *Comp. Struct.* **2018**, *202*, 590–602. [CrossRef]
46. Allaeys, F.; Luyckx, G.; Van Paepegem, W.; Degrieck, J. Characterization of real and substitute birds through experimental and numerical analysis of momentum, average impact force and residual energy in bird strike on three rigid targets: A flat plate, a wedge and a splitter. *Int. J. Imp. Eng.* **2017**, *99*, 1–13. [CrossRef]
47. Lin, J.; Naceur, H.; Coutellier, D.; Abrate, S. Numerical modelling of the low-velocity impact of composite plates using a shell-based SPH method. *Meccanica* **2015**, *50*, 2649–2660. [CrossRef]
48. Lin, J.; Guan, Y.; Li, J.; Huang, L.; Naceur, H.; Coutellier, D. Meshless modelling of low-velocity impacting damage for composite laminates. *Ferroelectrics* **2018**, *527*, 93–106. [CrossRef]
49. Guo, Q.; Gou, Y.; Chen, J.; Zhang, Y.; Zhou, Y. Dynamic response of foam concrete under low-velocity impact: Experiments and numerical simulation. *Int. J. Imp. Eng.* **2020**, *146*, 103693. [CrossRef]

50. Birnbaum, N.K.; Francis, N.J.; Gerber, B.I. Coupled Techniques for the Simulation of Fluid-Structure and Impact Problems. *Comput. Ass. Mech. Eng. Sci.* **1999**, *6*, 295–311.
51. Saputo, S.; Sellitto, A.; Riccio, A.; Di Caprio, F. Crashworthiness of a Composite Wing Section: Numerical Investigation of the Bird Strike Phenomenon by Using a Coupled Eulerian-Lagrangian Approach. *J. Mater. Eng. Perform.* **2019**, *28*, 3228–3238. [CrossRef]
52. Bedon, C.; Santi, M.V. Vulnerability and Structural Capacity Assessment of Historic Glass Facades under Bird-Strike. *Math. Prob. Eng.* **2022**, *2022*, 6059466. [CrossRef]
53. Zhang, X.; Hao, H. The response of glass window systems to blast loadings: An overview. *Int. J. Protect. Struct.* **2016**, *7*, 123–154. [CrossRef]
54. Bedon, C.; Louter, C. Exploratory numerical analysis of SG-laminated reinforced glass beam experiments. *Eng. Struct.* **2014**, *75*, 457–468. [CrossRef]
55. Mc Callum, S.C.; Constantinou, C. The Influence of Bird-Shape in Bird-Strike Analysis. In Proceedings of the 5th European LS-DYNA Users Conference, Birmingham, UK, 25–26 May 2005.
56. Hedayati, R.; Ziaei-Rad, S. A new bird model and the effect of bird geometry in impacts from various orientations. *Aer. Sci. Tech.* **2013**, *28*, 9–20. [CrossRef]
57. Cwiklak, J. Influence of a bird model shape on the bird impact parameters. *Facta Univ. Ser. Mech. Eng.* **2020**, *18*, 639–651. [CrossRef]
58. Georgiadis, S.; Gunnion, A.J.; Thomson, R.S.; Cartwright, B.K. Bird-strike simulation for certification of the Boeing 787 composite moveable trailing edge. *Comp. Struct.* **2008**, *86*, 258–268. [CrossRef]
59. Johnson, A.F.; Holzapfel, M. Modelling soft body impact on composite structures. *Comp. Struct.* **2003**, *63*, 103–113. [CrossRef]
60. Smojver, I.; Ivančević, D. Bird strike damage analysis in aircraft structures using Abaqus/Explicit and coupled Eulerian Lagrangian approach. *Comp. Sci. Tech.* **2011**, *71*, 489–498. [CrossRef]
61. Valdi, M.H.T.; Atrechian, M.R.; Shalkoohy, A.J.; Chavoshi, E. Numerical Investigation of Water Entry Problem of Pounders with Different Geometric Shapes and Drop Heights for Dynamic Compaction of the Seabed. *Geofluids* **2018**, *2018*, 5980386. [CrossRef]
62. Ahmadzadeh, M.; Saranjam, B.; Fard, A.H.; Binesh, A. Numerical simulation of sphere water entry problem using Eulerian-Lagrangian method. *App. Math. Model.* **2014**, *38*, 1673–1684. [CrossRef]
63. Bedon, C.; Santarsiero, M. Laminated glass beams with thick embedded connections—Numerical analysis of full-scale specimens during cracking regime. *Comp. Struct.* **2018**, *195*, 308–324. [CrossRef]
64. Martens, K.; Caspeele, R.; Belis, J. Numerical investigation of two-sided reinforced laminated glass beams in statically indeterminate systems. *Glass Struct. Eng.* **2016**, *1*, 417–431. [CrossRef]